Electromagnetic Laboratory Scientific Report No. 93

Design of a Low Side Lobe Short Series-fed Linear Array of Microstrip Patches

A. BENALLA and K. C. GUPTA

October, 1987

Department of Electrical and Computer Engineering
University of Colorado
Boulder, Colorado 80309-0425

Table of Contents

SUMMARY

This report describes a computer-aided procedure developed for design of linear series-fed arrays of rectangular microstrip patches. The radiating elements in the array are two-port rectangular microstrip patches with the input and output ports located along the non-radiating edges. A fraction of the power radiated from each element (and that transmitted to the next element) is controlled by the locations of the two ports and the width of the patch.

Analysis and design of the individual pathces is carried out by using a multi-port network model consisting of planar segments for the patch and the input-output transmission lines, an edge admittance network, and a mutual coupling network. A multiport network approach is also used for evaluating the voltage distribution at the radiating edges of the various elements of the array. This voltage distribution is expressed as an equivalent magnetic current distribution and is used for the evaluation of the radiation characteristics of the array.

ACKNOWLEDGEMENTS

This report forms a part of an exploratory development research project sponsored by the Department of the Navy (Contract NAVY N60530-84-C0095). The CAD software developed has been described separately in a software documentation report (SDR-1, September 1987) for the sponsors.

Several helpful discussions with Professor David Chang, co-principal investigator of the project, and Mr. Richard Chew, technical monitor from the Naval Weapons Center, China Lake, California, are gratefully acknowledged.

List of Symbols

a	antenna's length
b	antenna's width
B_e	effective width of the antenna
BW	linear array beamwidth
c_o	speed of light
d	array interelement spacing
D	array directivity
f	operating frequency
G_R	radiation conductance
G_S	surface wave conductance
h	thickness of dielectric substrate
k_0	free space wavenumber
L_1/L_2	input/output transmission line length
N	number of array elements
N_C	number of ports along both radiating edges
N_D	number of ports along input feed junction
N_P	number of ports along output feed junction
P_{in}	net time average input power
P_{rad}	fraction of input power radiated by the antenna
P_{loss}	fraction of input power dissipated as ohmic losses (conductor and dielectric)
S_{11}	input reflection coefficient
S_{21}	transmission coefficient

SLL	array side lobe level in (dB)
X_1/X_2	location of input and output feed along the non-radiating edges.
V_e	voltage along the radiating edges
Z_C	antenna impedance matrix
Z_V	matrix relating voltage at the radiating edges to the currents flowing at the input/output ports
$Z_0(1)/Z_0(2)$	characteristic impedance of the input/output transmission line
α	uniform progressive phase along the array
α'	ratio of radiation conductance to surface wave conductance
β	propagation constant of a transmission line
ϵ_r	relative dielectric constant of the substrate
θ_0	direction of the array main beam
tan δ	dielectric loss tangent

List of Figures

List of Tables

I. Phase and Amplitude Distributions in a Linear Array

This chapter is a brief review of linear antenna array concepts. Synthesis of a linear array using approximate expressions is described. The array elements are assumed to be identical. The effects of the element pattern on array performance can thus be accounted for by multiplying the array factor with the element pattern. In this chapter, the array factor is calculated for two types of linear arrays.

1.1 Length of Array from Gain/Beamwidth Specification:

The array length is determined either from the antenna directive gain or from the half power beamwidth BW specifications. For linear arrays, a very good working relation between directivity and beamwidth BW is [1, p.157]

$$D = 101.5^{o} / BW \qquad (1\text{-}1)$$

The directivity D is given by $10 \log_{10} D = g$, where g is the directive gain in dBs. The array length L is related to the directivity D by [1, p.155] :

$$L / \lambda_0 = D / 2 \qquad (1\text{-}2)$$

where λ_0 is the free space wavelength.

For a given directivity, expression (1-2) gives the minimum array length for any distribution with uniform progressive

phase.

1.2 Interelement Spacing and Number of Elements:

The only constraint on the uniform interelement spacing is to avoid the appearance of a second main beam (grating lobe). For this purpose, we require then that [1, p.125],

$$d / \lambda_0 < 1 / (1+| \cos(\theta_0) |) \qquad (1\text{-}3)$$

where θ_0 is the main beam direction measured from the direction of the array axis as shown in Fig.1-1.

The number of elements N is given by :

$$N = \mathrm{INT} [L / d] \qquad (1\text{-}4)$$

where INT [x] is the integer part of x.

1.3 Phase Distribution:

The linear array is assumed to have a uniform progressive phase. The phase is related to the main beam pointing direction θ_0 by:

$$\alpha = - k_0 \, d \cos (\theta_0) \qquad (1\text{-}5)$$

where k_0 is the free space wavenumber and d is the inter-element center to center spacing.

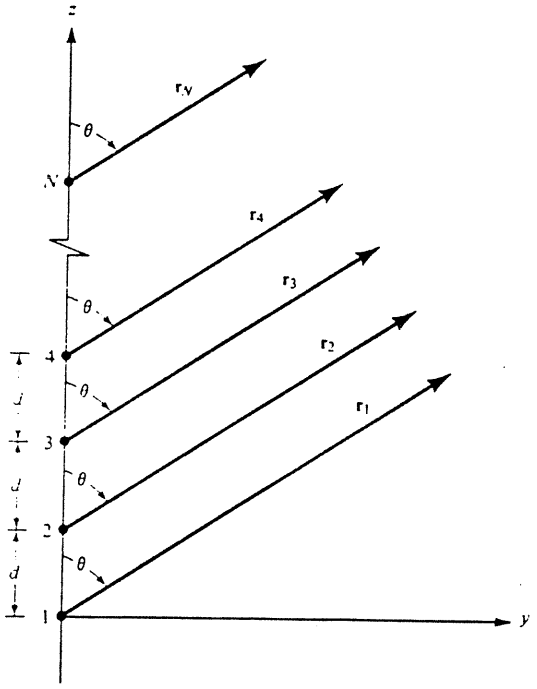

Fig.1.1 Far field geometry of N-element array of isotropic sources positioned along the z-axis

For a beam pointing at 30° from broadside ($\theta_0 = 60°$), α = $-k_0 d/2$, which (for $d = \lambda_0/2$) is equal to -90°.

1.4 Amplitude Distribution:

To achieve a low side lobe level SLL, the amplitude distribubution (power radiated from each element) needs to be adjusted properly. The two types of amplitude distributions which are commonly used for the design of linear array with low side lobe level are discussed next.

1.4.1 Chebyshev Distribution:

This type of amplitude distribution yields patterns with uniform side lobes. In this case, the relative amplitude distribution is given as follows:

a) For an array with N = 2M+1 elements, the amplitude of exitation to the n-th element (I_n) is given by [1, p.147]

$$I_n = \sum_{p=n}^{M} (-1)^{M-p} \frac{M}{M+p} \binom{M+p}{2p} \binom{2p}{p-n} U_0^{2p} \qquad (1\text{-}6)$$

where

$$\binom{N}{n} = \frac{N!}{(N-n)!\,n!}, \quad n = 0,M$$

b) For an array with 2M elements [1, p.147]

$$I_n = \sum_{p=n}^{M} (-1)^{M-p} \frac{2M-1}{2(M+p-1)} \binom{M+p-1}{2p-1} \binom{2p-1}{p-n} U_0^{2p-1} \qquad (1\text{-}7)$$

In both of the above expressions, U_0 is the solution of :

$$\cosh\{ (N-1) \cosh^{-1}(U_0) \} = b \qquad (1\text{-}8)$$

where b is related to the side lobe level SLL by :

$$20 \log_{10} b = \text{SLL (side lobe level in dBs)} \qquad (1\text{-}9)$$

Subroutine TCHEBYS in program ARSYNT listed in report SDR1 [7] uses relations (1-6) through (1-9) to compute the amplitude distribution for an array of N elements for any specified side lobe level.

The directivity D of a linear Chebyshev array [1, p.155] is :

$$D = \frac{2b^2}{1 + (b^2 - 1) \cdot (\lambda_0 / L) \cdot f} \qquad (1\text{-}10)$$

where f is called the beam broadening factor (relative to the uniform distribution case), and is related to SLL by [2, p.254]

$$f = 1. + .636\left\{\frac{2}{b} \cosh[\sqrt{(\cosh^{-1} b)^2 - \pi^2}]\right\} \qquad (1\text{-}11)$$

All other parameters have been defined previously. The half

power beamwidth BW of a Chebyshev array is related to the half power beamwidth BW_0 of a uniform array as:

$$BW = BW_0 \cdot f \tag{1-12}$$

1.4.2 Taylor distribution:

In this type of amplitude distribution for arrays, the close-in side lobes are required to be below a given level. The side lobes which are further out are at increasingly lower levels. For usual practical parameter values, the beam broadening associated with the choice of close-in side lobes to be below a prescribed level is negligible.

The determination of element excitations is carried out using the null matching technique [1]. The pattern of an array with 2M + 1 elements, $f_0(w)$ in the w-space, is given by [1,177]:

$$f_0(w) = \sum_{n=0}^{2M} \binom{I_n}{I_N} W^n = \prod_{n=1}^{2M} (W - W_n) \tag{1-13}$$

where W_n denotes zeros for $f_0(w)$ and is related to U_n by [1, p.173]

$$W_n = e^{j2\pi U_n / N} \tag{1-14}$$

where U_n is a null in the pattern [1, p.160]

(1-15)

$$U_n = \begin{cases} \pm n\, A\left[\dfrac{A^2 + (n-\frac{1}{2})^2}{A^2 + (N_A-\frac{1}{2})^2}\right] & 1 \le n < N_A \\ \pm n & N_A \le n \le M \end{cases}$$

where cosh (A) = b , and $20 \log_{10} b$ = SLL (dB).

I_n denotes the amplitude of excitation to the n-th element. N_A is the number of close-in side lobes whose levels are below SLL. In practice, N_A is chosen to be between 2 and 6. The half power beam width BW for Taylor array [2] is :

(1-16)

$$BW = 2 \sin^{-1}\left\{ \frac{\lambda_0 \alpha_1}{\pi L} \sqrt{(\cosh^{-1} b)^2 - (\cosh^{-1} b/\sqrt{2})^2} \right\}$$

where

$$\alpha_1 = N_A / \sqrt{A^2 + (N - 1/2)}$$

where the directivity of the array is related to the BW by (1-1).

Subroutine TAYLOR in program ARSYNT [7], uses relations (1-13) through (1-15) to compute the amplitude distribution for (2N + 1) element array with specified N_A and SLL.

Remark: For the array design example discussed later in Section 4.1, Taylor distribution is used for amplitude distribution of the various elements.

II. Series-Fed Linear Array

In this chapter, various types of feed arrangements are briefly reviewed.

2.1 Feed Structures:

This section describes different practical forms of feed arrangements for distributing input power to various elements of a linear array. The methods of feeding presented are applicable to all types of linear arrays. Only feed networks located on the upper surface of the substrate (which contains the radiating array elements) are discussed.

1. Series Feed

This arrangement is by far the simplest form of feed system. The radiating elements are connected together by intervening section of transmission lines as shown in Figure 2-1. The lengths of these transmission line sections are chosen so as to achieve the required phase distribution.

The power is fed to the array either at its center or at one of its ends. A fraction of the input power to each element is radiated, and the rest (minus losses) is transmitted to the next element. Thus, each element in the array (except possibly the last one) has two transmission lines connected to it. Additional design flexibility is obtained when the array is terminated by a matched load. The transmission coefficient of each element is adjusted suitably in order to achieve a specified amplitude distribution.

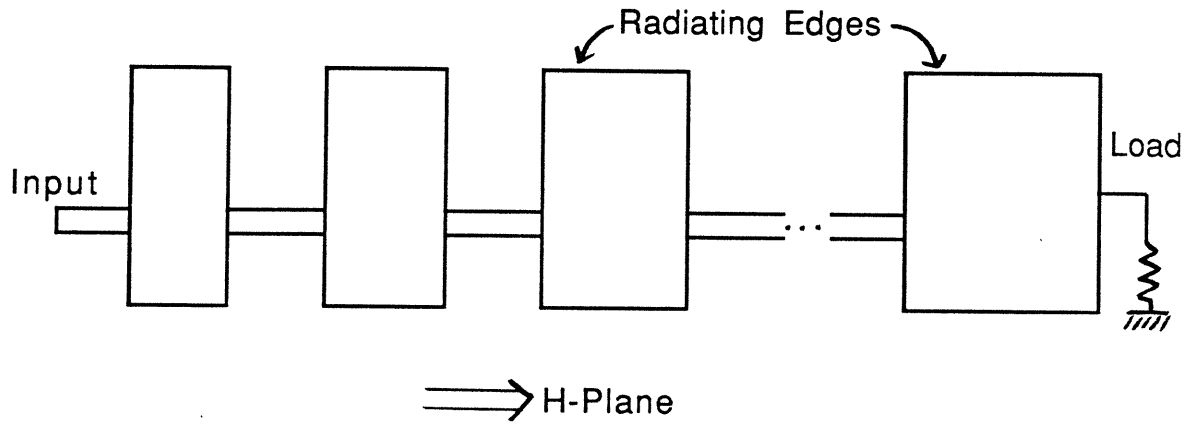

Fig 2-1-a Series fed array of microstrip patches with the polarization plane perpendicular to the array axis.

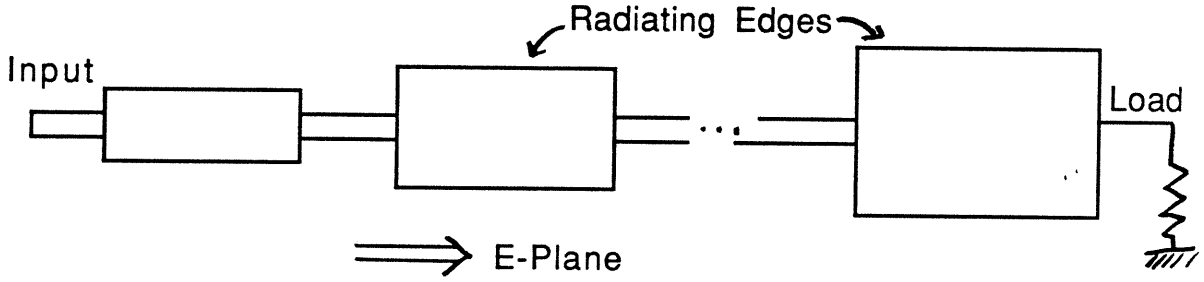

Fig 2-1-b Series fed array of microstrip patches with the polarization plane parallel to the array axis .

The orientation of the elements in the array (Fig. 2.1a and Fig. 2.1b) determines the polarization of the radiated wave.

When the frequency changes, the progressive phase shift along a series-fed array changes, which causes the main beam to change direction (or to split for a center-fed case). For a center-fed array structure, the input power is inserted into the array at a location near the elements which radiate maximum power. This reduces the line losses and results in higher efficiency .

2. Series Compensated Feed

In using this type of feed arrangement (shown in Fig. 2-2), the line lengths are adjusted such that the array is frequency insensitive and the beam pointing direction does not shift when the frequency is changed. This is because the path lengths from the input to various elements in the array are equal. Unlike the series-fed array, all array elements are single-port patches in this case.

3. Corporate (or parallel) Feed

In this case, the input power is distributed to each element in the array by use of power splitters as shown in Fig. 2-3. For a broadside array, the path lengths between the feed and various elements are maintained equal. The space required to implement this type of feed increases for an increasing number of array elements. A specified amplitude distribution is achieved by changing the impedance of transmission lines in the power dividers. All radiating elements are single-port patches in

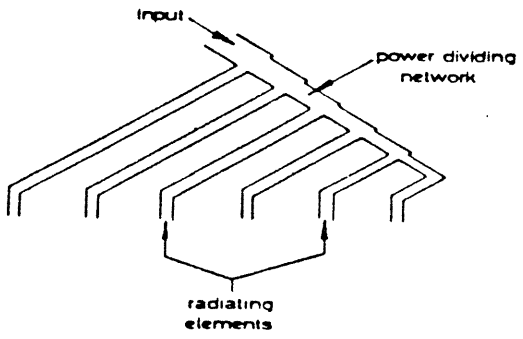

Fig 2-2 Series compensated feed

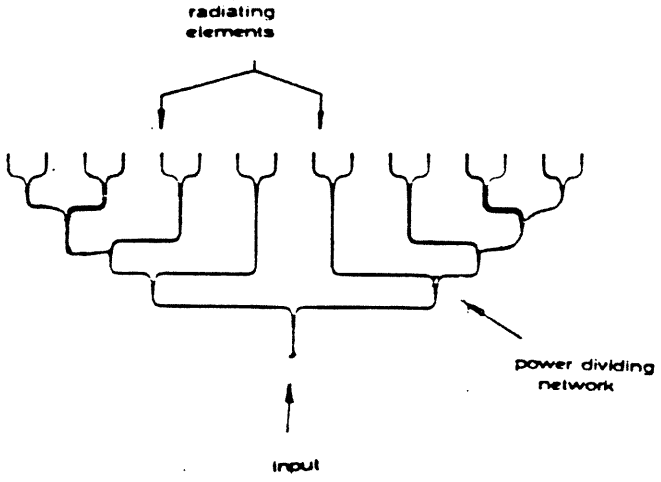

Fig. 2-3 Corporate parallel feeding network

this case also.

4. Comparison of Feed Systems [3]

The efficiency of an array (using any type of feed) is decreased by increasing the transmission line length between the input and the array elements. A summary of advantages and disadvantages of the three types of feed arrangements discussed above is given in Table 2-1.

For the design discussed in the report, a series-fed linear array is selected due to the following considerations:

(i) lower feed line losses, and

(ii) restriction on the space available in a direction transverse to the array axis.

2.2 S-Parameters For Cells of a Series-Fed Array (lossless case):

In the design of a linear series fed array, it is necessary to know the transmission characteristics of each unit cell in the array. A typical cell in the array consists of a radiating element characterized by its impedance matrix plus halves of the line lengths connecting it to its neighboring elements (as shown in Fig. 2-4). The two lines are characterized by their lengths L_1 and L_2 and their characteristic impedances $Z_0(1)$ and $Z_0(2)$. When the mutual coupling among the array elements is negligible, the array design reduces to the design of the individual cells. The requirement on the S-parameters of each radiating element in order to achieve a specified aperture distribution are discussed in this section.

Table 2-1 Comparison of Feed Networks

feed type	main beam direction	bandwidth	limiting parameters	efficiency	space usage
1) Series feed					
A. Travelling wave					
a) End fed	frequency insensitive	wide	pattern*	moderate to high	efficient
b) center fed	//	narrow	/ /	better than end fed	/ /
B. Resonant array					
a) end fed	/ /	very narrow	VSWR	moderate to high	/ /
b) center fed	/ /	/ /	/ /	better than end fed	/ /
2) series compensated	broadside frequency independent	wide	pattern	moderate to high	moderate
3) corporate feed	/ /	/ /	/ /	/ /	poor

(// indicates same as above)

* beam direction and SLL

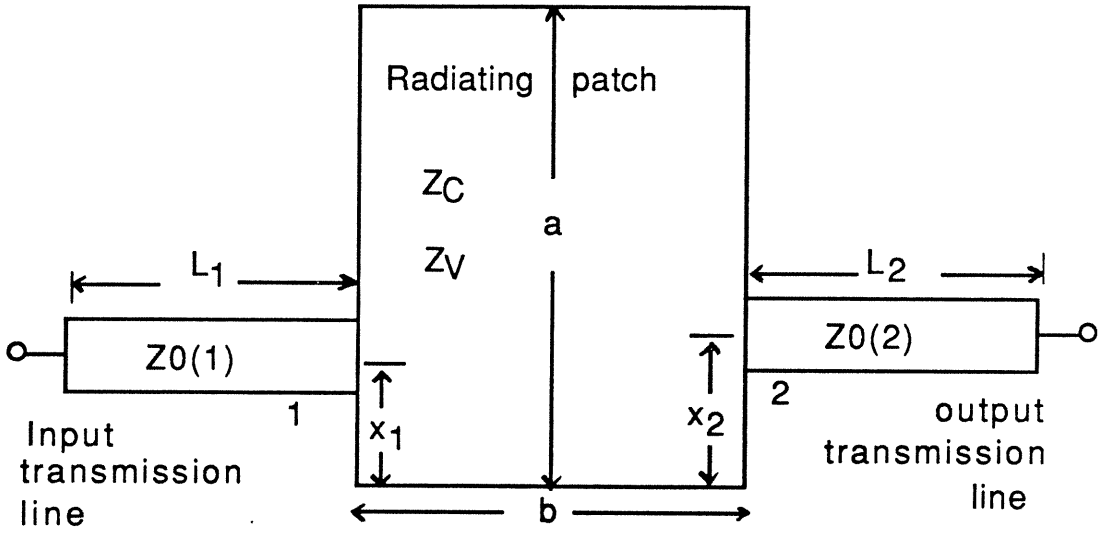

Fig.2.4 Typical unit cell in the array

2.2.1 Input Reflection Coefficient:

To obtain an impedance match at the input of the array, we require that every cell element in the array be matched at its input port. This input match at the individual elements ensures that the phase and amplitude of the radiation from each element are controlled by the input signal only and not by the signal reflected back from the next element.

2.2.2 Transmission Coefficient:

To achieve a specified amplitude distribution along the array aperture, the radiated power from each array element needs to be controlled. The corresponding requirements on the transmission coefficients S_{21} of array elements are discussed for two cases separately. The lossless case is considered first. The lossy case is discussed in Section 2.3.

In the lossless case, the input power to each element is divided into radiated power and power transmitted to the next element of the array. The fractional power transmitted to the next elements is given by $|S_{21}|^2$.

A method of computing $|S_{21}|$ for each radiating element for a specified amplitude distribution is given below.

The input power to the array may be written as :

$$P_{in} = \sum_{i=1}^{M} C^2(i) + P_L \qquad (2\text{-}1a)$$

where M is the total number of elements in the case of an end-fed linear series array or half the number of elements in a center-fed array. (Each half is fed in series.) C(i) is the relative amplitude of the radiation of the i^{th} array element, C_i^2 being the power radiated.

P_L is the amount of power dissipated in the matched load connected at the far end of the array. This arrangement can be used to increase the array bandwidth and, to some extent, to make the array elements more similar. If P_L is chosen to be equal to a fraction of the input power P_{in} ($P_L = P_{in}$), then the input power to the array may be written

(2-1b)

$$P_{in} = \frac{1}{1-\gamma} \sum_{L=1}^{M} C_i^2$$

The power radiated from each element, normalized to the input power (P_{in} (i)) to that element, may be written

(2-2

$$P_{rn}(i) = C(i)^2 / P_{in}(i), \qquad 1 \le i \le M$$

(2-3)

where

$$\begin{cases} P_{in}(i) = P_{in} - \sum_{d=1}^{i-1} C(j)^2, & 2 \le i \le M \\ P_{in}(1) = P_{in} \end{cases}$$

where P_{in} is the total input power fed to the array.

The magnitude of the transmission coefficient $|S_{21}|$ for the i^{th} radiating element is obtained as

$$|S_{21}(i)| = \sqrt{1 - P_{rn}(i)} \qquad 1 \le i \le M \tag{2-4}$$

Subroutine POWER in programs STANDAR and ANTV4 in [7] is used to compute the required transmission coefficients for each of the unit cells in the series-fed linear array.

In the case of a series-fed array without any load at the far end, the last element is a single port and the only requirement for this element is that $S_{11} = 0$.

The lengths of the interelement transmission line sections are dependent on the S-parameters of the radiating elements and are determined from the uniform progressive phase α (needed for the beam to point in a specified direction) by :

$$\beta l = -\alpha + \text{Ang}(S_{21}) + \text{Ang}(V_e(i+1))_a - \text{Ang}(V_e(i))_a \tag{2-5}$$

where

$$\beta = \omega \cdot \sqrt{e_{re}(f)}/\, c$$

and ε_{re} (f) is the effective dielectric constant of the microstrip line taking dispersion into account. The angle α is the uniform progressive phase ($-2n\pi \le \alpha \le 0$), needed to point

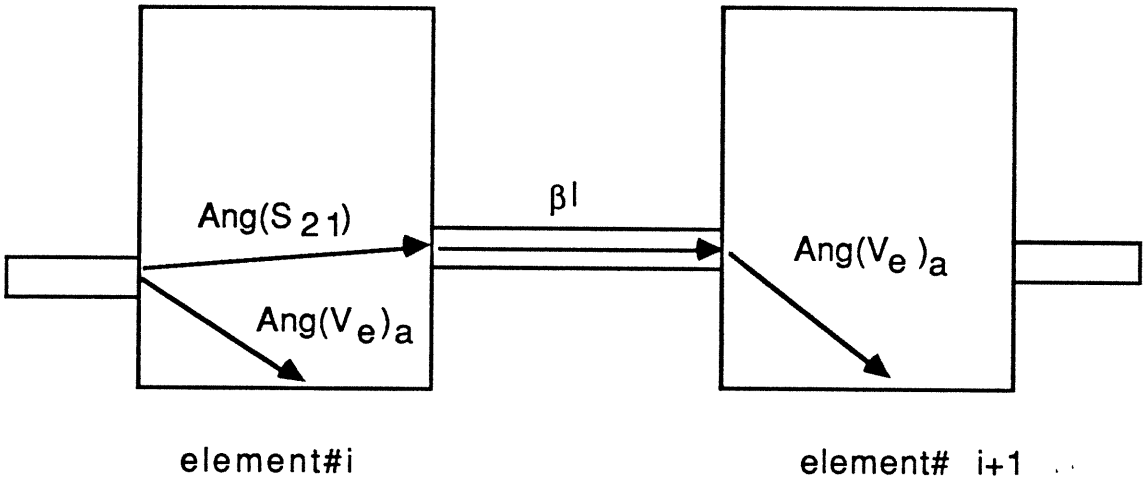

Fig. 2-5 Phase relationship between edge voltages in two adjacent unit cells of the array.

the radiated beam in a specified direction.

Ang (S_{21}) is the phase delay of the transmission through the i^{th} element referred to its input and output ports as shown in Fig. 2-5. $Ang(V_e(i))_a$ is the average phase of the value of the voltages at the radiating edge of the i^{th} element (nearer to the input port) with respect to its input port (Fig. 2-5).

It may be noted that the value of output reflection coefficient S_{22} is not involved in this calculation.

2.3 S-Parameters of Array Cells in Lossy Case:

The losses in microstrip antenna arrays can be divided into three types: dielectric, conductor, and surface wave losses. These losses are dependent on the dimensions of the elements. The requirements on the reflection coefficients S_{11} (to be zero) remain the same as in the lossless case. These array losses must be taken into account in determining the amplitudes of the transmission coefficients. A procedure for finding $|S_{21}|$ in the case of a lossy array is discussed next.

The input power P_{in} given in (2-1) is now equal to:

$$P_{in} = \sum_{i=1}^{M} (C(i)^2 + P_{loss}(i)) + P_L \qquad (2\text{-}6)$$

where $P_{loss}(i)$ is the total power loss in the i^{th} cell (radiating element plus half lengths of the interconnecting transmission lines). Other parameters have been defined earlier.

The input power $P_{in}(i)$ used in (2-3) is now equal to

$$P_{in}(i) = P_{in} \sum_{j=1}^{i-1} (C(j)^2 + P_{loss}(j)) \tag{2-7}$$

The transmission coefficient of the i^{th} cell in the array is

$$|S_{21}(i)| = \sqrt{1 - \varepsilon(i) - (1 + \alpha')P_{rn}(i)} \tag{2-8}$$

where $\varepsilon(i)$ is defined as the sum of the dielectric and conductor power losses as a fraction of the power input to the i^{th} element.

$$\varepsilon(i) = (P_{diel}(i) + P_{cond}(i)) / P_{in}(i) \tag{2-9}$$

α' is the ratio of surface wave power to the power radiated from the same element. To the first approximation, α' is independent of the element dimensions [ ] and is given in Section 3-3 :

$$\alpha' = P_{surf} / P_{rad} \tag{2-10}$$

Expression (2-6) for the input power to the array is

expressed in terms of C(i), ϵ(i), γ, and α' as

(2-11)

$$P_{in} = \left(\sum_{i=1}^{M} d(i)C^2(i)\right) / \ (1 - \gamma - S)$$

where

$$d(i) = (1 + \alpha') - \sum_{j=i}^{M} b(j,i)$$

$$b(j,i) = \epsilon(j)\left[(1 + \alpha') - \sum_{k=i}^{j-1} b(k,i)\right]$$

$$S = \sum_{i=1}^{M} a(i)$$

$$a(i) = \epsilon(i)\left[1 - \sum_{j=1}^{j-1} a(j)\right]$$

$$a(i) = \epsilon(i)$$

$$b(i,i) = 0$$

2.4 Iterative Computation of $|S_{21}|$ in the Lossy Case

As mentioned in Section 2-3, the losses depend on the design of element cells, but the computation of power to be radiated from each cell and the cell design to achieve the corresponding $|S_{21}|$ require the knowledge of the losses in the various cells of the array. Thus, the design of the array has to be done using an iterative procedure. The first step in this procedure is to design the array cell elements assuming no losses. Then the losses associated with each of the elements are computed, and the array elements are redesigned using those computed losses. The losses in the redesigned array elements are computed and used as the

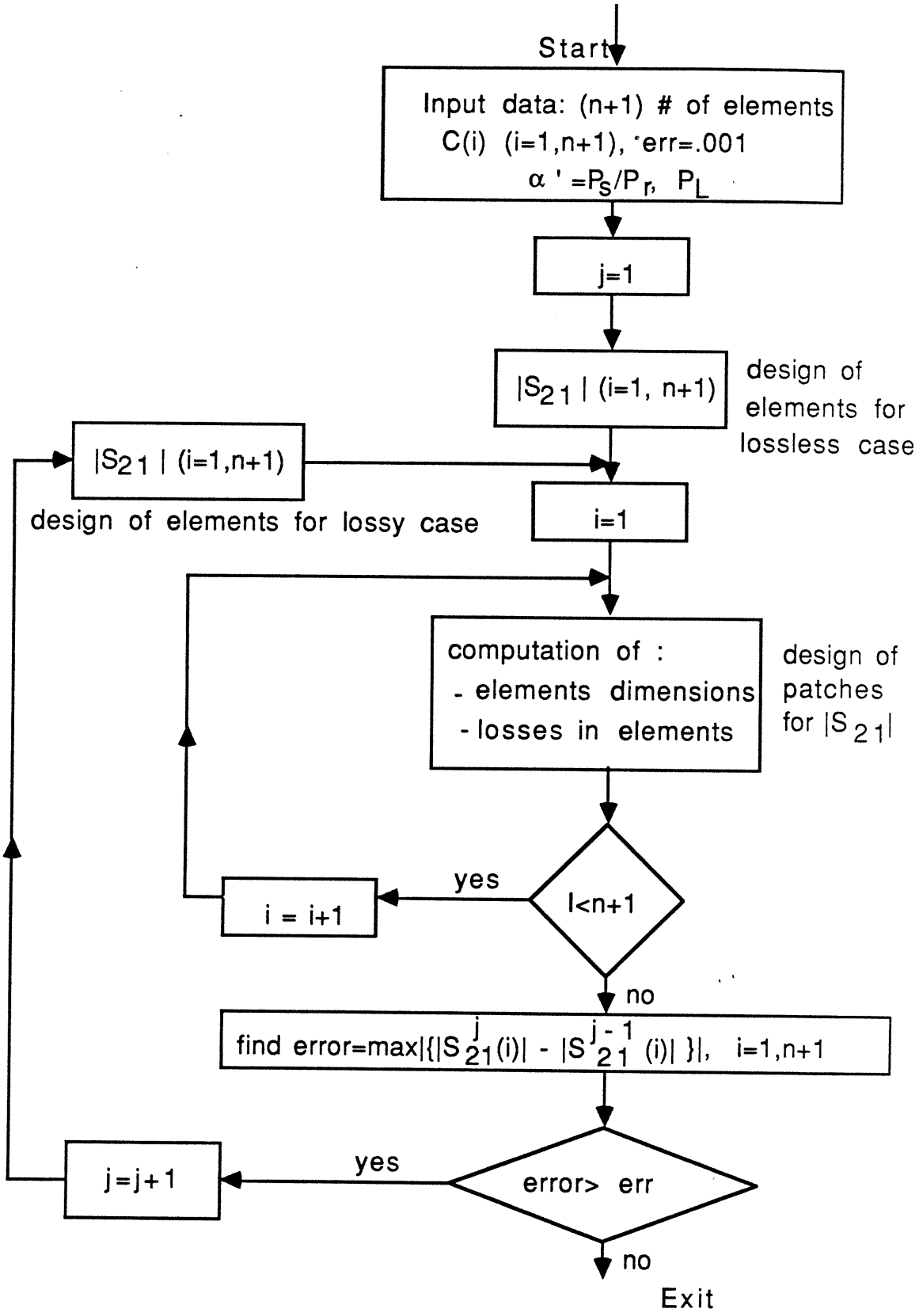

Fig 2-6 Flow chart for iterative computation of $|S_{21}|$ in the lossy case.

new starting values for redesigning the array elements. The flow chart shown in Fig. 2-6 summarizes the different steps needed in the array design in the lossy case. In this flow chart j is the number of iterations. The iteration process is terminated when the difference between computed losses in two successive steps is within a prescribed value err. It may be noted that the losses are not very sensitive to the element dimensions, so the number of iterations needed is small (typically three or four).

Subroutine PLOSSES in program ARSYNT in [7] is used to compute $|S_{21}|^2$ of each unit cell of the lossy series-fed linear array.

III. Design of Two-Port Patches

3.1 Analysis By Segmentation Method:

Segmentation method is a network approach for analysis of planar antenna (or circuit) configurations wherein the con-figuration is divided into simpler segments, each segment is characterized separately, and these individual characterizations are combined together to obtain the characteristics of the overall antenna (or circuit) config-uration. This method can be used for microstrip patch antennas on thin substrates.

3.1.1 Segments of a Two-Port Patch:

For microstrip patches on thin substrates, we can separate description of internal fields underneath the patch and ex-ternal fields associated with fringing from the edges, the radiation and the surface waves. The internal fields are characterized by treating the patch as a planar network with multiple ports around the periphery. A Z-matrix characteri-zation of such a multiport model of the patch can be obtained from the Green's function for the patch geometry (rectangu-lar, circular, triangular, etc.). Since these Green's functions relate the E-field (or voltage) to the current, a Z-matrix representation is convenient. For this reason, we use Z-matrix representations for other segments (edge admit-tance networks, etc.) also.

A multiport network model of a cell of the linear array being discussed here is shown in Fig. 3-1. Segment A is a planar

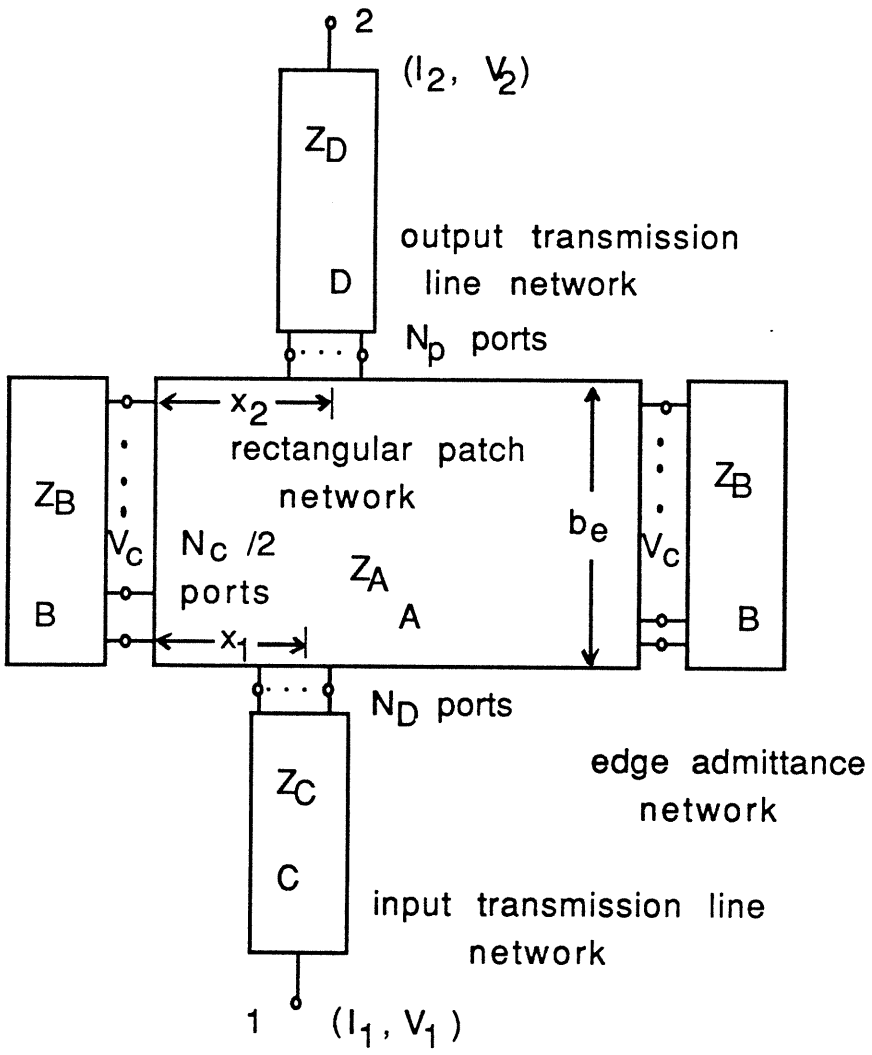

Fig. 3-1 A multiport network representation of a two-port rectangular microstrip antenna.

component representing the internal fields of the patch. The Z-matrix of this segment may be obtained as discussed later in Section 3.2.

Segment B represents the external fields associated with the two radiating edges of the patch in terms of an edge admittance network (EAN). Modelling of this network is discussed in Section 3.3.

Segments A and B are interconnected at a discrete number of points along the radiating edges. The number of these connecting ports is decided by the field distribution along the radiating edges. If there is no variation of the field along the radiating edges, only one interconnection would be needed. However, because of the assymmetry caused by the input and output ports and, because of the operation of the antenna slightly away from the resonance of the dominant mode, a larger number (typically five) of interconnections is needed at each edge.

Mutual coupling between the two radiating edges can also be modelled in terms of a network called mutual coupling network (MCN). With this network incorporated, the multiport network model of a cell of the array appears as shown in Fig. 3-2 .

It may be noted that the edge admittance networks of Fig. 3-1 have been included in the MCN shown in Fig. 3-2. The modelling of the mutual coupling network is discussed in

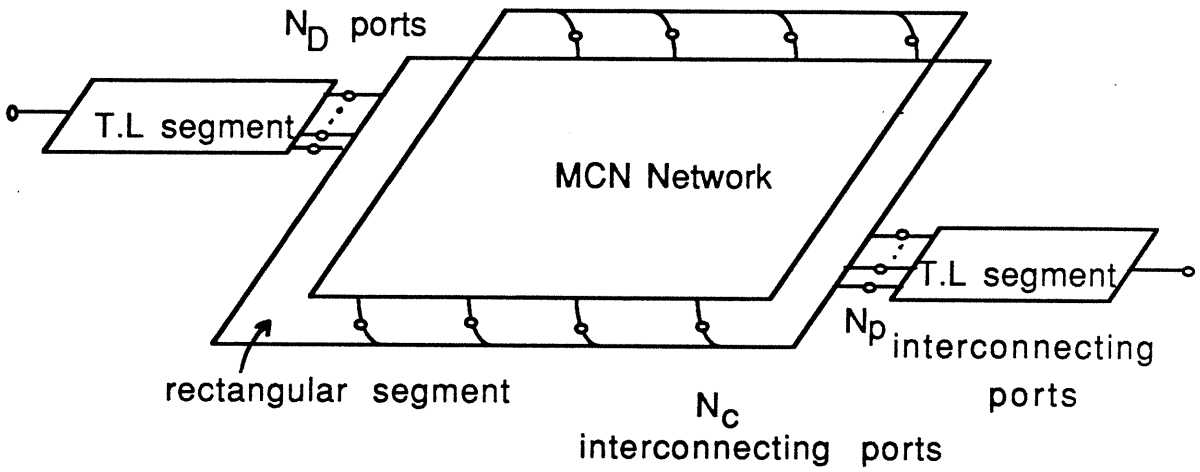

Fig 3-2 Multiport Network Model of a unit cell with mutual coupling network included.

3.1.2 Combining Segments:

Having obtained the Z-matrices for various segments, the overall Z-matrix with respect to ports 1 and 2 can be obtained by segmentation formula [4]. The segmentation technique may be illustrated by combining two segments A and B (Fig. 3-3) with impedance matrices Z_A and Z_B to yield the segment C (Fig. 3-4) with an impedance matrix Z_C .

A reduction in computational effort will be achieved if the connected ports (denoted by q for segment A and by r for segment B) are suitably regrouped [4]. This is done in such a way that q_1 and r_1 ports are connected together, q_2 and r_2 are connected together, and so on. The external ports for each segment (denoted by p_1 for A and by p_2 for B) are numbered first. Thus, the impedance matrices for the two segments A and B can be written together as:

$$\begin{bmatrix} V_p \\ V_q \\ V_r \end{bmatrix} = \begin{bmatrix} Z_{pp} Z_{pq} Z_{pr} \\ Z_{qp} Z_{qq} Z_{qr} \\ Z_{rp} Z_{rq} Z_{rr} \end{bmatrix} \cdot \begin{bmatrix} I_p \\ I_q \\ I_r \end{bmatrix} \qquad (3\text{-}1)$$

where the different submatrices can be written more explicitly as

$$Z_{pp} = \begin{bmatrix} Z_{p1p1} & Z_{p1p2} \\ Z_{p2p1} & Z_{p2p2} \end{bmatrix}$$

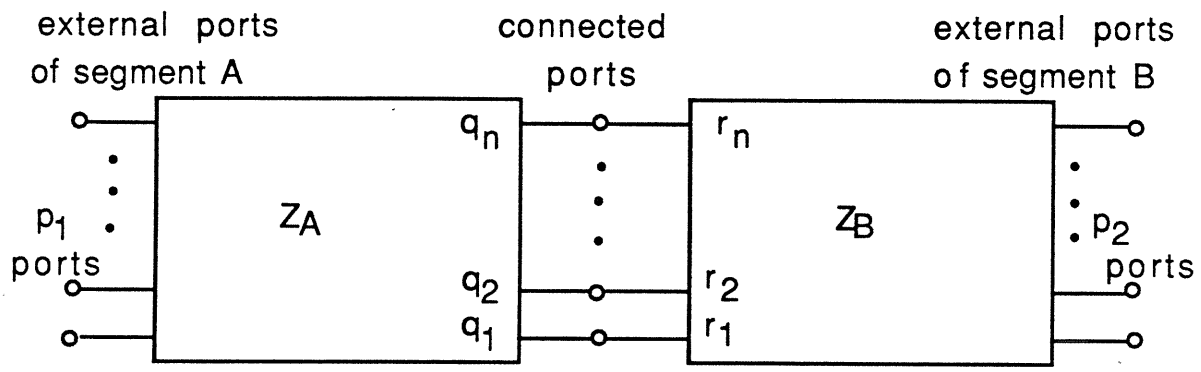

Fig 3-3 Two multiport network segments.

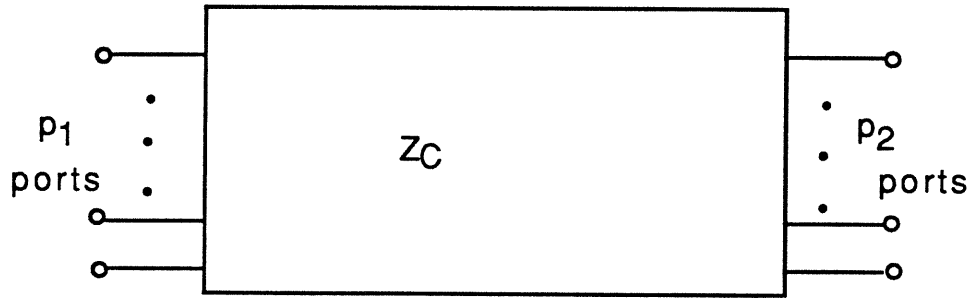

Fig 3-4 Overall multiport network segment.

$$Z_{pq} = \begin{bmatrix} Z_{p1q} \\ 0 \end{bmatrix}$$

$$Z_{pr} = \begin{bmatrix} 0 \\ Z_{p2r} \end{bmatrix}$$

and where $p = p_1 + p_2$, $q = r$. V and I represent the voltage and current at different ports.

Using the interconnection constraint that the voltages at any two connected ports be equal and that the sum of the currents there be zero, the Z-matrix of the segment C is given by [4].

$$Z_c = Z_{pp} + (Z_{pq}-Z_{pr})(Z_{qq}+Z_{rr})^{-1} \cdot (Z_{rp} - Z_{qp}) \qquad (3\text{-}2)$$

The voltages V_q at the connected ports q are related to the currents I_p flowing at the external ports p by:

$$V_q = Z_v I_p \qquad (3\text{-}3)$$

$$Z_v = [Z_{qp} + (Z_{qq} - Z_{qr})(Z_{qq} + Z_{rr})^{-1} \cdot (Z_{rp} - Z_{qp})]$$

Equations (3-2) and (3-3) are the fundamental working relations in the segmentation method.

Subroutine SEGMENT in programs STANDAR and ANTV4 [7] is used for the implementation of the segmentation method discussed above.

3.2 Rectangular Segments:

3.2.1 Z-matrix of Rectangular Segments:

The elements of the Z-matrices of the rectangular segment A and the transmission lines C and D are obtained from the Green's function [5] .

Case a: The two ports q and p (Fig. 3-5) are oriented along the same direction. The corresponding element of the Z-matrix is obtained as

(3-4)

$$Z_{pq} = -CF\frac{1}{n}\sum_{\ell=0}^{L}\sigma_\ell \cos(k_u u_p)\cos(k_u u_q)\cos(\gamma_\ell z_>)\cos(\gamma_\ell z_<)$$
$$\cdot\frac{\mathrm{sinc}(\frac{k_u w_p}{2})\,\mathrm{sinc}(\frac{k_u w_q}{2})}{\gamma_\ell \sin\gamma_\ell F} - jCF\frac{1}{n}\sum_{\ell=L+1}^{\infty}\cos(k_u u_q)\cos(k_u u_p)$$
$$\mathrm{sinc}(\frac{k_u w_p}{2})\,\mathrm{sinc}(\frac{k_u w_q}{2})\,\frac{\exp(-j\gamma_\ell(v_> - v_<))}{\gamma_\ell}$$

where

$$(v_>, v_<) = \begin{cases} (y_>, y_<), & \ell = m \\ (x_>, x_<), & \ell = n \end{cases} \qquad \gamma_\ell = \pm\sqrt{k^2 - k_u^2}$$

$$k_u = \begin{cases} \frac{m\pi}{a}, & \ell = m \\ \frac{n\pi}{b}, & \ell = n \end{cases} \qquad F = \begin{cases} b, & \ell = m \\ a, & \ell = n \end{cases}$$

$$(z_>, z_<) = \begin{cases} (y_>-b, y_<), & \ell = m \\ (x_>-a, x_<), & \ell = n \end{cases} \qquad (u_p, u_q) = \begin{cases} (x_p, x_q), & \ell = m \\ (y_p, y_q), & \ell = n \end{cases}$$

$$\sigma_m = \begin{cases} 1, & m = 0 \\ 2, & m \neq 0 \end{cases}$$

$k^2 = \omega^2\mu\varepsilon_0\varepsilon_r(1 - j\delta)$, $C = j\omega\mu d/(ab)$, and δ equals the loss tangent of the dielectric.

Case b: When the two ports p and q are oriented in different directions x and y, the expression for Z_{pq} becomes

(3-5)

$$Z_{pq} = -CF\frac{1}{n}\sum_{\ell=0}^{L}\sigma_\ell\cos(k_u u_p)\cos(k_u u_q)\cos(\gamma_\ell z_<)\cos(\gamma_\ell z_>)$$
$$\cdot\frac{\operatorname{sinc}(\frac{k_u w_i}{2})\operatorname{sinc}(\frac{\gamma_\ell w_j}{2})}{\gamma_\ell \sin\gamma_\ell F} - CF\frac{1}{n}\sum_{\ell=L+1}^{\infty}\cos(k_u u_p)\cos(k_u u_q)$$
$$\operatorname{sinc}(\frac{k_u w_i}{2})\frac{\exp(-j\gamma_\ell(v_> - v_< - \frac{w_j}{2}))}{\gamma_\ell^2 w_j}$$

The choice of dummy variable ℓ (either m or n) is made by noting that, for fast convergence of the above summation, it is required that $(v_> - v_< - w_j/2) > 0$.

The choice of L is a compromise between fast convergence and accuracy. In practice, L is chosen such that $\gamma_\ell F \leq 500$ (for Cyber 720/170 computer systems. For VAX 780 systems, $\gamma_\ell F \leq 50$.) The sign in front of the square root is chosen such that the imaginary part of γ_ℓ is negative.

Function ZZ2 in [7] uses the above expressions to compute the elements of the Z-matrix of a rectangular planar component.

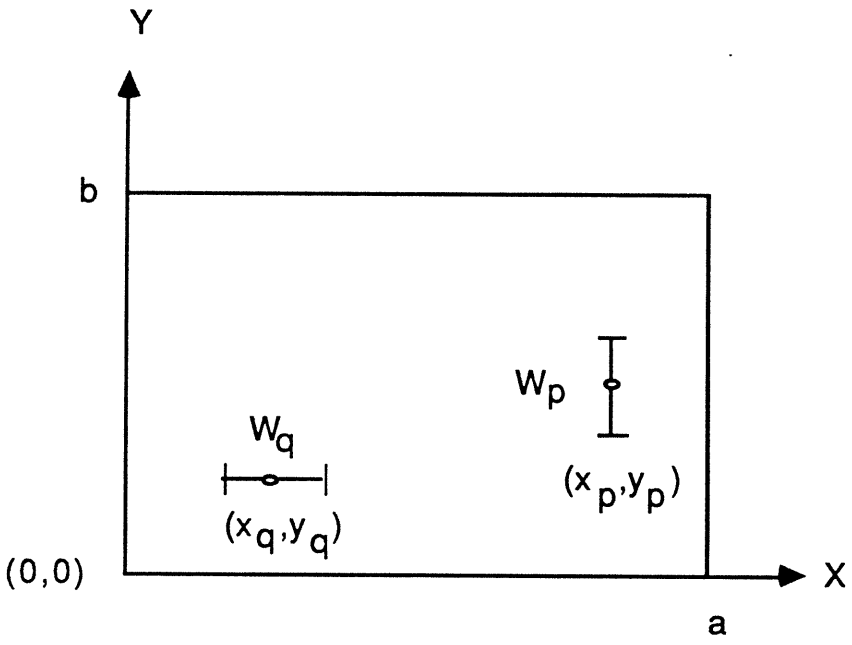

Fig. 3-5 Ports locations and their relative orientations in a planar rectangular component.

3.2.2 Rectangular Patch Segment:

This segment is a multiport rectangular planar component with dimensions a and b_e and magnetic wall boundaries around its periphery. The effective width b_e is introduced in place of physical width b to account for the effects of fringing fields along the non-radiating edges of length a. We also use an effective dielectric constant $\varepsilon_{re}(f)$ to account for the fields being partially in the substrate and partially in the air region and to account for effects of dispersion at the operating frequency f. The size of the matrix Z_A, which characterizes this segment, is $(N_c + N_d + N_p) \cdot (N_c + N_d + N_p)$. N_c denotes the number of interconnected ports between the rectangular and the edge admittance (or MCN) segments. The typical value used for N_c is 8. N_d and N_p denote the number of interconnected ports between the patch and the input and output transmission line segments.

A typical value for N_d and N_p is $N_d=N_p=5$. The elements of the matrix Z_A are computed using the results of Section 3.2.1. In numerical computations, the infinite series of Section 3.2.1 are truncated, and a value of L = 100 yields very good accuracy.

Subbroutine RRES in programs STANDAR and ANTV4 [7] is used to compute the Z-matrix of the rectangular patch.

3.2.3 Transmission Line Segments:

Segments C and D in Fig. 3-I represent small sections of microstrip lines connected to the input and output ports of the patch. These line sections are considered as planar rectangular components in order to account for the effects of any higher order evanescent modes that may be excited by the discontinuity at the junctions between the patch and the input/output lines. The equivalent rectangular components of these segments have effective widths W_{e1}, W_{e2} and effective dielectric constants $\varepsilon_{re1}(f)$, $\varepsilon_{re2}(f)$ corresponding to the two microstrip lines. The transmission line lengths L_1, L_2 are assumed to be long enough that the higher order evanescent modes decay out and only the TEM mode is present at the external ports. L_1, L_2 should typically be at least 0.1 λ_0. Since the effective widths of the microstrip lines are not very small and since the ports are located at the non-radiating edges, the voltage along the interface between the patch and the input or output line is not constant. Therefore, we need more than one port at this interface. It has been found [6] that a value of interconnected ports N_D=N_P equal to 5 yields good accuracy. The $(N_D + 1) \cdot (N_D + 1)$ Z-matrices characterizing these segments are also obtained from formulas given in Section 3.2.1 by letting $b_e = w_{e1}$ or w_{e2} and $\varepsilon_{re}(f) = \varepsilon_{re1}(f)$ or $\varepsilon_{re2}(f)$ respectively for segments C and D.

Subroutine EFFECT in [7] is used for the computation of the Z-matrices of the transmission line segments.

3.3 Edge Admittance Network:

The edge admittance matrix Y_{ee} characterizing the EAN's, represents the radiated power, power coupled to surface waves, and fringing fields associated with the two radiating edges of the rectangular microstrip patch antenna. When each edge of effective width b_e is divided into $N_C/2$ sections, the admittance matrix Y_{ee} is an (N_C x N_C) matrix. This matrix has all non-diagonal elements equal to zero, and those along the principal diagonal are given by:

$$Y_{ee}(i,i) = 2(G_R + G_S + jB) / N_C \qquad (3\text{-}6)$$

G_R, the radiation conductance for each radiating edge, is computed by using an equivalent magnetic line source [3] and is given by

(3-7)

$$G_R = \begin{cases} b_e^2 / 90\lambda_0^2 & b_e < .35\lambda_0 \\ b_e / 120\lambda_0 - 1/60\pi^2 & .35\lambda_0 \le b_e \le 2\cdot\lambda_0 \\ b_e / 120\lambda_0 & 2\cdot\lambda_0 < b_e \end{cases}$$

where λ_0 is the free space wavelength. G_S is the surface wave conductance and is related to the radiation conductance by [3, p. 56]

(3-8a)

$$\frac{G_R}{G_S} = \frac{\cos^2(k_{y1}h)\epsilon_r(k_{y1}h)^2}{\cos^2(k_{y1}h)\epsilon_r(k_{y2}h)^2 + (k_{y1}h)^2(k_{y2}h)}$$

where

$$\begin{cases} k_{y1}^2 + k_{y2}^2 = k_0^2(\varepsilon_r - 1) \\ \tan(k_{y1}h) = \varepsilon_r k_{y2} / k_{y1} \end{cases}$$

or

$$(k_{y1}h)^2 = (k_0 h)^2 \varepsilon_r^2 (\varepsilon_r - 1) / \{ \varepsilon_r^2 + \tan^2 (k_{y1}h) \} \quad (3\text{-}8b)$$

Expression (3.8b) is a transcendental equation for $k_{y1}h$ and is solved using numerical methods. h denotes the height of the substrate and k is the free space wave number $= \omega\sqrt{\mu_0 \in_0}$

B is the edge susceptance which represents the effect of fringing fields at the two open ends (radiating edges of the patch). Using the equivalent parallel plate waveguide model, B is given by [8]

$$B = \omega b/2 \{\varepsilon_{re}(f)/c_0 Z_0 \text{ (air)} - \varepsilon_0 \varepsilon_r a/h\} \quad (3\text{-}9)$$

$$c_0 = 3 \times 10^8 \text{ m/s}$$

and Z_0 (air) is the characteristic impedance of a microstrip line where width = a and ε_r=1. Formulas for design calculation of microstrip lines are included in the appendix. $\varepsilon_{re}(f)$ is the effective dielectric constant of an equivalent microstrip line of width a. An empirical expression using half dispersion is found to give better agreement between

theoretical and measured resonant frequency. We use

$$B = \{B(\varepsilon_{re}(0)) + B(\varepsilon_{re}(f))\}/2 \qquad (3\text{-}10)$$

Subroutine ZF in [7] is used for the evaluation of the self edge admittance.

3.4 Mutual Coupling Network:

The mutual coupling network accounts for the external interaction between the two radiating edges of the microstrip patch. It also is convenient to absorb the two edge admittance networks (EAN's) in the mutual coupling network.

The mutual coupling admittance between the two edges describes the current induced at one edge due to a unit magnetic current line source at the other edge. When the antenna is operating in the dominant mode, the voltages at the two radiating edges are 180° out of phase and the electric field distribution will be as shown in Fig. 3-6a. For evaluation of the external field (which causes mutual coupling), the equivalence principle is used to replace the field at the aperture by a pair of equivalent magnetic line sources (Fig. 3-6b). Since the height of substrates used is small, the ground plane can be removed, and the magnitudes of the magnetic current line sources are doubled to account for the presence of image sources.

For the computation of the mutual coupling admittance matrix, we make use of the basic expression for the fields

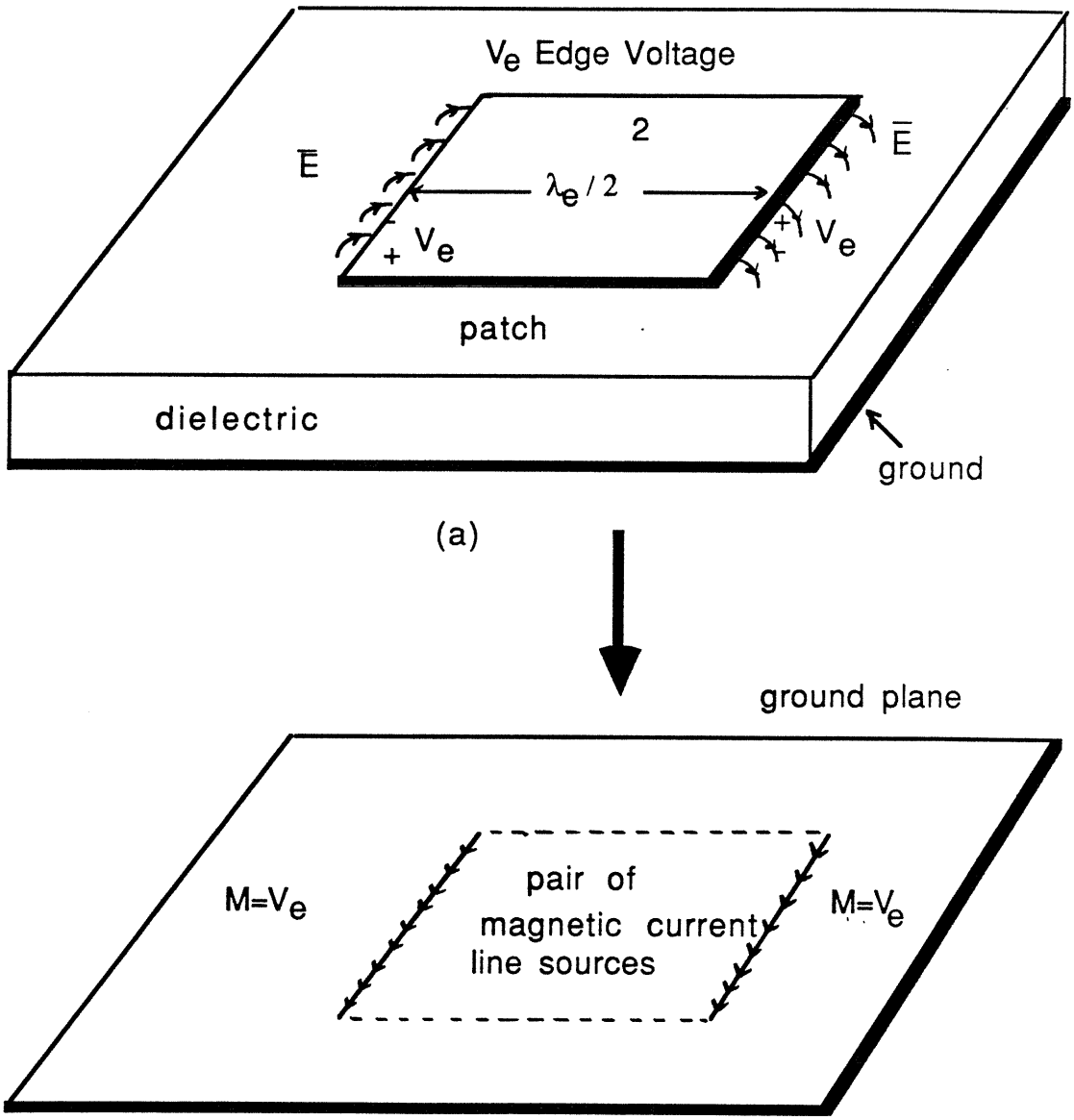

Fig 3-6 Equivalent line souces for the computation of mutual coupling.

produced by a magnetic dipole in free space. The magnetic field components H_θ and H_r of a magnetic dipole of moment Mdl in free space (as shown in Fig. 3-7) are given by

$$H_\theta = j \frac{k_0 M\, dl \sin\theta}{4\pi\eta_0 r} \left\{ 1 + \frac{1}{jk_0 r} - \frac{1}{(k_0 r)^2} \right\} e^{-jk_0 r} \tag{3-11}$$

$$H_r = \frac{M\, dl \cos\theta}{2\pi\eta_0 r^2} \left\{ 1 + \frac{1}{jk_0 r} \right\} e^{-jk_0 r} \tag{3-12}$$

The magnetic field of a magnetic dipole oriented arbitrarily in the X–Y plane as shown in Fig. 3-8 may be written as

$$\begin{aligned} H_x &= H_y' \sin(\theta_i) + H_x' \cos(\theta_i) \\ H_y &= H_y' \cos(\theta_i) - H_x' \sin(\theta_i) \\ H_x' &= H_\theta \cos(\theta) + H_r \sin(\theta) \\ H_y' &= -H_\theta \sin(\theta) + H_r \cos(\theta) \end{aligned} \tag{3-13}$$

The mutual admittance between two magnetic dipole sources of moments $M_i dl_i$, $M_j dl_j$ located at x_i, y_i and x_j, y_j respectively (with arbitrary orientation in space) as shown in Fig. 3-8 is given by

$$Y_{ji} = J_j\, dl_j / M \tag{3-14}$$

where J_j is related to the magnetic field H produced by M_i at (x_j, y_j) by

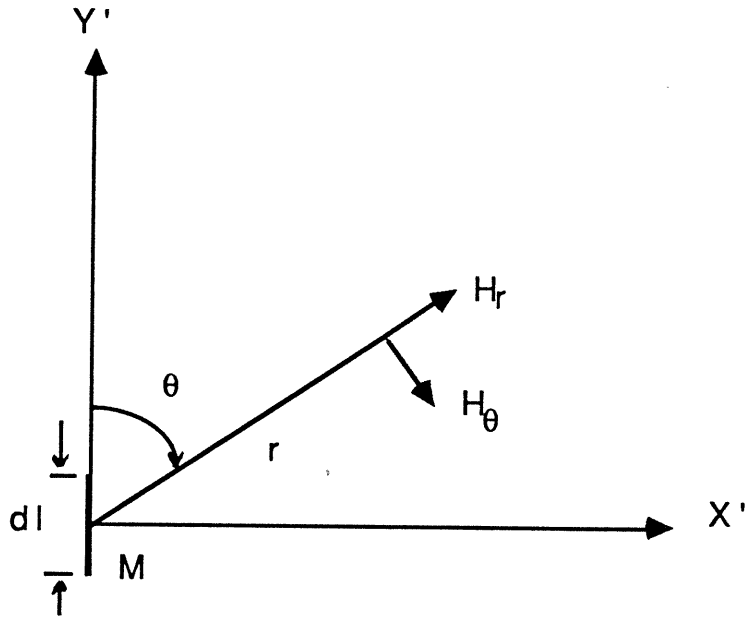

Fig. 3-7 Coordinate system for the computation of the field of a magnetic dipole.

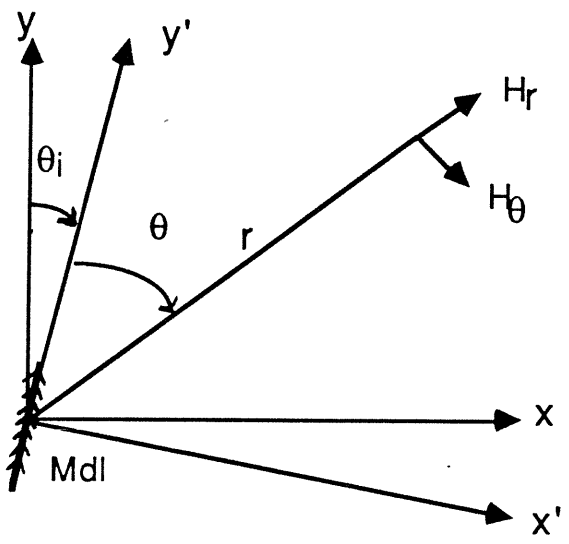

Fig 3-8 Magnetic dipole arbitrarily oriented in the X-Y plane.

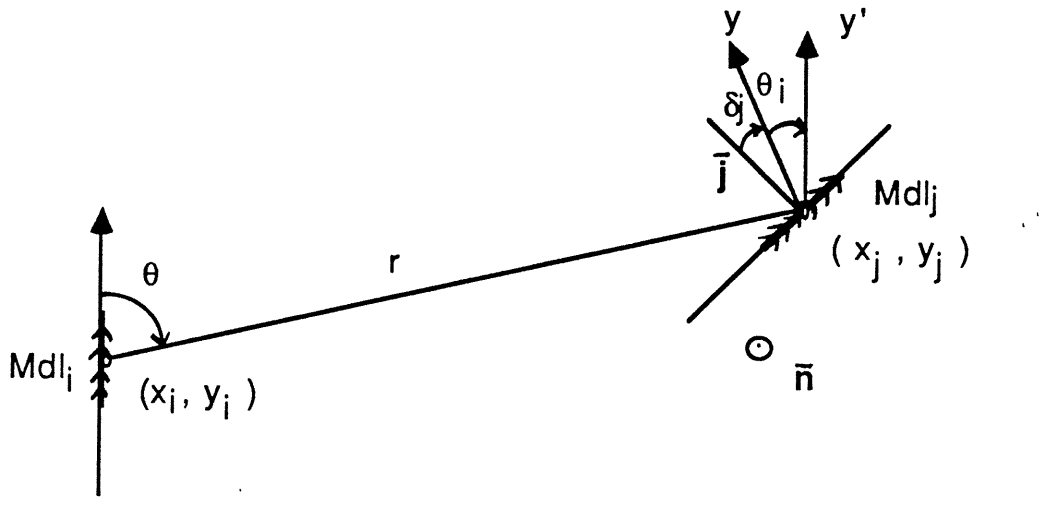

Fig.3-9 Mutual coupling between two arbitrarily oriented linear magnetic currents in the x-y plane.

$$J_j = 2(\bar{n} \times \bar{H})\bar{j} \qquad (3\text{-}15)$$

$$= - H_x \cos(\delta_j) - H_y \sin(\delta_j)$$

where $\bar{n}$ is the normal to the plane of the patch. $\bar{j}$ is a unit vector normal to the direction of the magnetic dipole at x_j, y_j as shown in Fig. 3-9. $r^2 = (x_j - x_i)^2 + (y_j - y_i)^2$ and (x_i, y_i), (x_j, y_j) are the coordinates of the locations of the two dipoles.

To use the result derived in (3-14), each edge of the rectangular patch is subdivided into a number (N) of sections (typically N =16). The mutual coupling is computed among the ports located at one edge and the ports located at the other edge. For a rectangular patch antenna, values of the angle θ_i and δ_j are shown in Fig. 3.10. The mutual admittance matrix Y can be expressed as

$$Y = \begin{bmatrix} 0 & Y_m \\ Y_m & 0 \end{bmatrix} \qquad (3\text{-}16)$$

The submatrix Y_m represents the mutual admittance between the two radiating edges. For N = 16, each Y_m matrix is 16 x 16.

In the multiport network approach, the dimensions of the matrix Y are reduced to a value equal to the number of ports chosen at the edges of the rectangular patch segment (N_c).

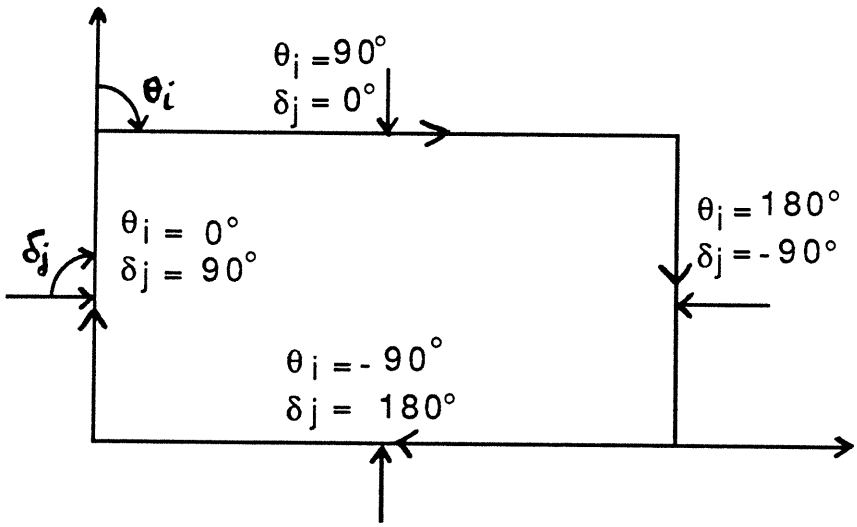

Fig. 3-10 Equivalent magnetic line current distribution for a unit voltage at the patch periphery.

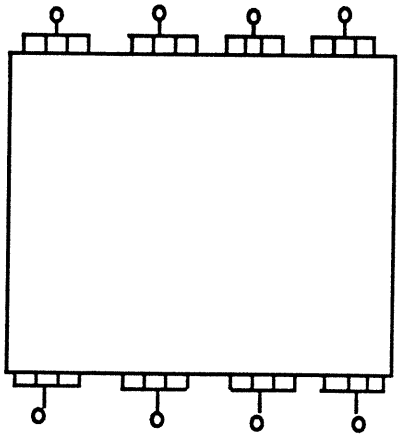

Fig3-11 Grouping of ports for reduction in the size of the mutual coupling admittance matrix.

The reduction in the size of matrix Y is carried out by connecting several adjacent ports together as shown in Fig. 3-11. This implies that the voltages at the combined ports are equal and that the current at the resulting port is the sum of the current flowing at the combined ports. The reduced matrix is an (N_c) x (N_c) matrix where N_c is the number of interconnected ports between the rectangular segment and the mutual admittance segment and is given by

$$Y_e = \begin{bmatrix} Y_{ee} & Y_{em} \\ Y_{em} & Y_{ee} \end{bmatrix} \tag{3-17}$$

The elements of the submatrix Y_{ee} were given in Section 3.3. The elements of the submatrix Y_{em} are computed from those of Y_m by

$$Y_{em}(i\,j) = \sum_{k=1}^{2N/N_c} \sum_{m=1}^{2N/N_c} Y_m\left(\frac{2N\,i}{N_c} - k + 1, \frac{2N\,j}{N_c} - m + 1\right) \tag{3-18}$$

where i,j = 1, . . . ,N_c and N is an integer multiple of N_c with large enough so that the double summation converges.

Subroutines COUPLE and REDUCE [7] are used for the evaluation of the elements of the mutual admittance matrix.

The above procedure may be used to evaluate mutual coupling between any two edges of the patches in an array. The effects of mutual coupling between non-radiating edges as

well as among non-radiating and radiating edges of the same patch are found to be small compared to the effect of mutual coupling between radiating edges [10]. In the design example considered in the next chapter, only mutual coupling between the radiating edges of the same patch is considered.

The effect of mutual coupling between the adjacent elements of the array is found to be small and is not included in the array design procedure discussed in the next chapter.

IV. Design of the Array

In this section, a step-by-step procedure for the design of a linear array is described. This procedure makes use of the design equations from the previous sections and of the corresponding computer programs listed in a separate report [7]. A flowchart outlining the sequence of various steps involved is shown in Fig. 4-1.

4.1 Array Specifications:

As an example of the use of the array design procedure described in this report, the design of a short series-fed array of rectangular microstrip patches, is discussed. The directive gain of the array is 13 dB. The side lobe levels are to be below 30 dB. The direction of the main beam is to be 30° off broadside. The array antenna will operate around a center frequency of f=7.5 GHz. The array is to be fabricated on 5880 Duroid substrate with dielectric constant $\varepsilon_r = 2.2$. The substrate thickness is h =1/64", and the dielectric loss tangent tanδ is 9.10^{-4}. The substrate is coated with 1/2 oz copper. For this example, we will consider no resistive load connected at the far end of the linear array.

4.2 Array Length and Number of Elements:

Using equation (1-2) relating the directive gain to the array length L, we have

$$L = D/2 \cdot \lambda_0 \qquad (4\text{-}1)$$

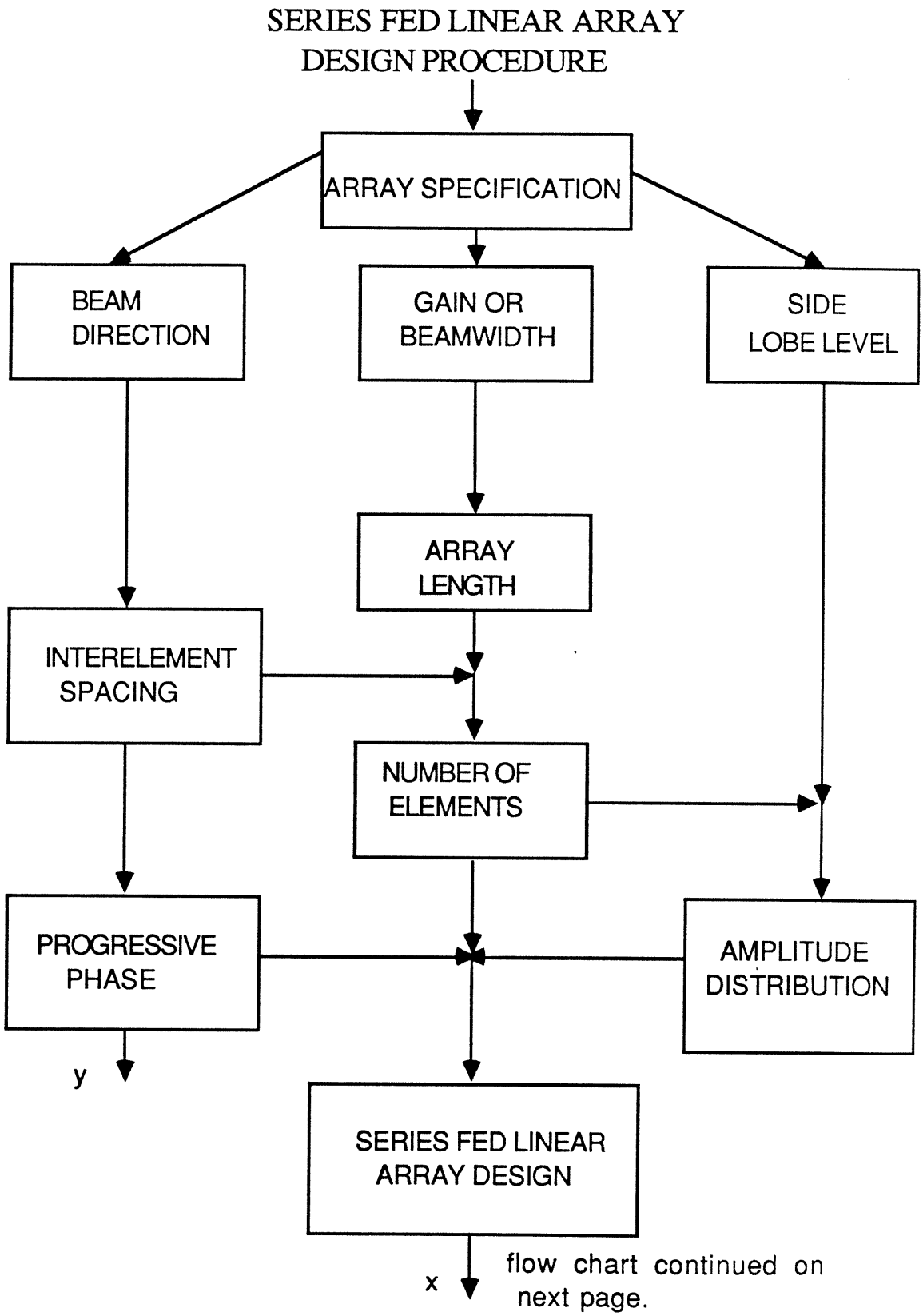

Fig 4-1 Flow chart for design of linear series fed array for both lossy and lossless cases.

SERIES FED LINEAR ARRAY DESIGN PROCEDURE (CONTINUE)

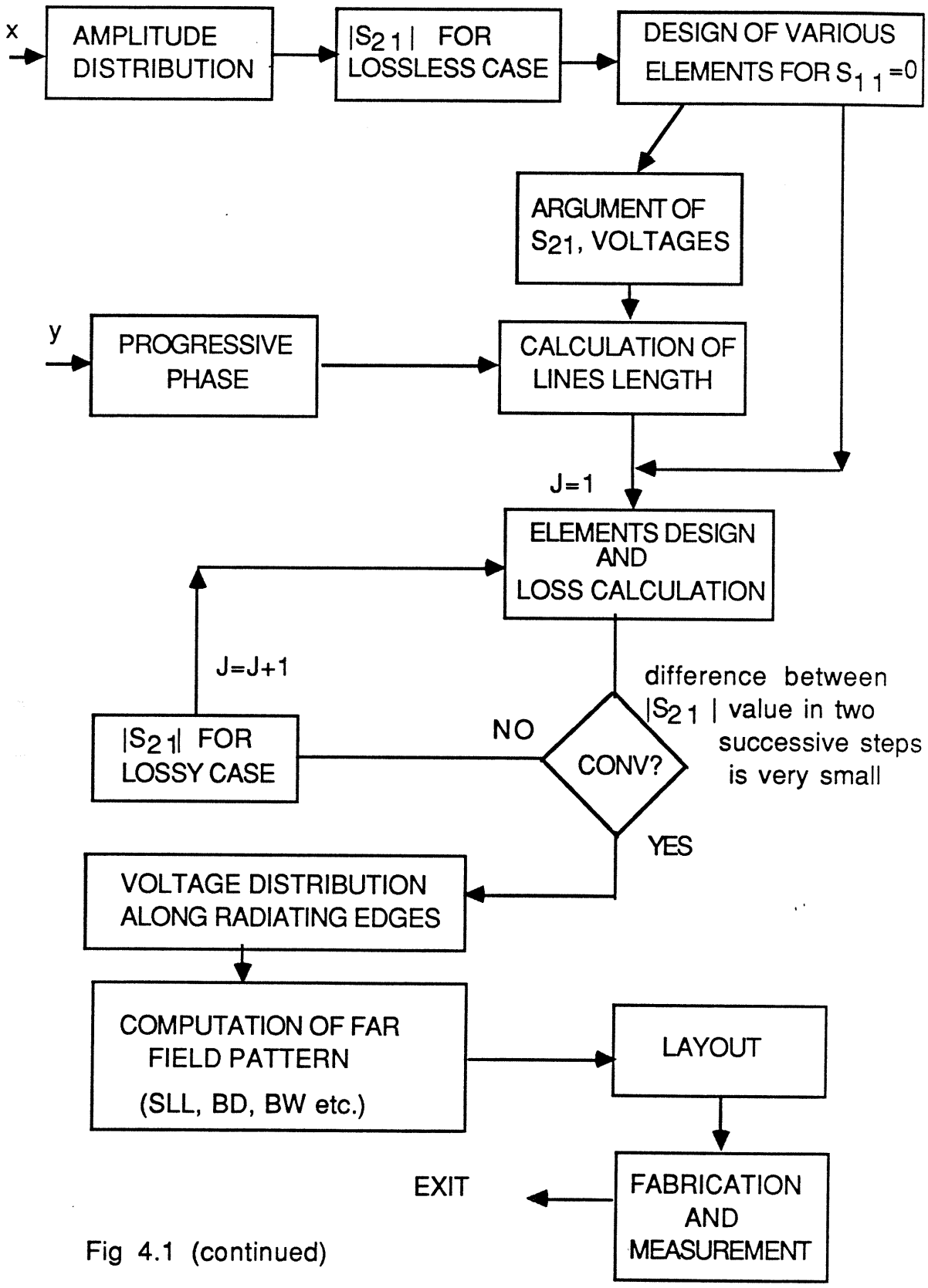

Fig 4.1 (continued)

where $10 \log_{10} D = 13$ and $D \cong 20$. This yields

$$L \cong 10 \lambda_0 \tag{4-2}$$

The element spacing is chosen to be

$$d = \lambda_0 / 2 \tag{4-3}$$

$\lambda_0/2$ spacing ensures that there are no grating lobes over the entire visible range. The spacing can be increased when we are interested in the beam over a limited range of directions only.

Using equation (1-4), the number of elements is

$$N = 19 \tag{4-4}$$

4.3 Array Aperture Distribution:

To achieve the 30 dB side lobe level and the 30° off broadside beam direction, the uniform progressive phase and the relative distribution must be properly selected.

4.3.1 Uniform Progressive Phase α:

Using relation (1-5), there are two possible values of α which result in a 30^o off broadside beam pointing:

$$d = \lambda_0/2 \Rightarrow \alpha = \begin{cases} -90^\circ & \text{for } \theta = 60^\circ \\ -270^\circ & \text{for } \theta = 120^\circ \end{cases} \quad (4\text{-}5)$$

The use of $\alpha = -90^\circ$ results in interconnecting transmission lines shorter than the spacing between elements (which is $\lambda_0/2$). So a differential phase shift $\alpha = -270^\circ$ is used. This requires the interconnecting line lengths to be longer than the spacing between patches. Curved interconnecting lines are used for connecting adjacent patches.

4.3.2 Relative Amplitude Distribution:

The linear array of nineteen elements, with side lobe level SLL = 30 dB, is designed using subroutine TAYLOR [7]. The parameter N_A is set equal to 6. The relative amplitude distribution, normalized to the excitation of the center element, has a symmetry around the center element and is given in Table 4-1.

4.4 Design of Array Elements:

The nineteen element linear series-fed array of rectangular microstrip patches is designed using the analysis technique discussed in Chapter 3. The elements are designed separately. The computation of $|S_{21}|$ for each element, so as to meet a required amplitude distribution of the array, depends on the losses in the element. Also, these losses cannot be computed until the element's dimensions are known. The first step in the design is to ignore losses in the array and

Table 4-1

RELATIVE AMPLITUDE DISTRIBUTION FOR TAYLOR ARRAY*

array elements	amplitude distribution normalized to the center element
1,19	.2664
2,18	.3048
3,17	.3900
4,16	.5112
5,15	.6384
6,14	.7531
7,13	.8536
8,12	.9343
9,11	.9840
10	1.000

$N_A = 6$, S.L.L. = 30 dB

* obtained from Subroutine TAYLOR in [7].

Table 4-2

$|S_{21}|^2$ DISTRIBUTION FOR LOSSLESS CASE AND NO LOAD*

array element #	$\|S_{21}\|^2$	array element #	$\|S_{21}\|^2$
1	.99232	11	.76505
2	.98987	12	.72323
3	.98325	13	.68052
4	.97073	14	.63454
5	.95298	15	.58621
6	.93132	16	.54736
7	.90526	17	.51858
8	.87465	18	.43322
9	.84103	19	0
10	.80475		

Taylor array with N_A = 6, S.L.L. = 30 dB

* obtained from subroutine POWER in program ARSYNT in [7]

compute the $|S_{21}|^2$ of each element using subroutine POWER in program ARSYNT [7]. With the square of amplitude distribution of Table 4-1 as input data for subroutine POWER, the computed $|S_{21}|^2$ distribution for the array example considered is shown in Table 4-2.

To design the nineteen element array of rectangular microstrip patches to meet the $|S_{21}|^2$ specification in Table 4-2, we make use of design tables listing two-port patch characteristics for various patch dimensions as shown in Tables 4-3 and 4-4. The introduction of this kind of table helps in speeding the design process. These tables yield a very good approximation of the dimensions of a patch to achieve a given $|S_{21}|$. Later in this section, we will present an example of a step-by-step design of a two-port patch for a given $|S_{21}|$. Table 4-3 shows the variation in $|S_{21}|$ of a two-port rectangular patch with given width as a function of the output port location x_2. As mentioned earlier, for the array configuration being considered both the input and output ports are located along the non-radiating edges. Table 4-4, on the other hand, shows the variation in $|S_{21}|$ of a two-port rectangular patch for a given x_2 as a function of the patch width b. The other design parameters a and x_1 are chosen such that the input reflection coefficient $S_{11} = 0$.

In the array design example being discussed here, a set of more detailed tables similar to Table 4-3 for two-port

Table 4-3

VARIATION OF TWO-PORT CHARACTERISTICS
WITH OUTPUT PORT LOCATION

x_2(cm)	x_1(cm)	a(cm)	$\|S_{21}\|^2$	$\angle S_{21}$°	P_{rad}	P_{loss}
.52	.457	1.3261	.5088	-18.6	.2672	.2235
.50	.442	1.3272	.5702	-18.4	.2327	.1967
.48	.426	1.3285	.6225	-18.5	.2033	.1739
.46	.409	1.3298	.6659	-18.5	.1788	.1549
.44	.391	1.3314	.7027	-18.6	.1582	.1388
.42	.373	1.3330	.7334	-18.8	.1409	.1254
.40	.355	1.3346	.7589	-18.9	.1265	.1143
.38	.336	1.3364	.7806	-19.1	.1143	.1048
.36	.316	1.3384	.7991	-19.4	.1039	.0968

b = 6 mm, ε_r = 2.2, h = 1/64"
Z0(1) = Z0(2) = 75 Ω, f = 7.5 GHz

Table 4-4

VARIATION OF TWO-PORT CHARACTERISTICS
WITH PATCH WIDTH

b(cm)	x_1(cm)	a(cm)	$\|S_{21}\|^2$	$\angle S_{21}$°	P_{rad}	P_{loss}
.55	.360	1.3388	.7815	-17.2	.1115	.1068
.50	.365	1.3437	.8041	-15.6	.0968	.0989
.45	.371	1.3495	.8422	-14.2	.0742	.0835
.40	.375	1.3567	.8484	-12.9	.0687	.0828
.35	.379	1.3651	.8695	-11.4	.0558	.0746
.30	.383	1.3760	.8898	-10.2	.0437	.0663
.25	.386	1.3896	.9089	- 8.9	.0328	.0582

x_2 = .4 cm, ϵ_r = 2.2, h = 1/64"
Z0(1)= Z0(2) = 75 Ω, f = 7.5 GHz

patches whose widths range from 0.1 mm to 8 mm (in increments of .5 mm) were created. Those tables are not shown here due to space limitation. The value of $|S_{21}|$ for other values of widths and input and output port locations are computed by using an extrapolation scheme. In all of these computations, both the input and output transmission line lengths are taken to be 1.0 cm long (0.25 λ_0). Also, the ratio of surface wave power loss to the power radiated (for the substrate parameters mentioned earlier) is found (from equation 3-8) to be $\alpha` = 1.7710^{-3}$.

As an example of the use of these tables, let us say that it is necessary to estimate the losses associated with the patch with $|S_{2|}|^2$ 0.7650. From Table 4-4, this value of $|S_{21}|^2$ lies between $|S_{21}|^2 = 0.7494$ and $|S_{21}|^2 = 0.7771$, so the estimated fractional loss may be taken as (0.0772 + 0.0702)/2 = 0.0737. To achieve the distribution shown in Table 4-2, the widths of the array elements are reduced gradually as we move along the array. In order to reduce the phase error related to unequal widths of adjacent patches (phase delay between the input port and the radiating edges), it is desirable to have the widths of adjacent patches as close as possible. In other words, the difference between two successive elements' widths has to be small ($\leq$ 1 mm). The elements having a smaller $|S_{21}|$ will have a larger width, and the elements having a larger value of $|S_{21}|$ will have a smaller width in the array.

With the above constraints imposed on the choice of element width, we select the values of $|S_{21}|$ from the design tables, which closely approximate the values of $|S_{21}|$ distribution of Table 4-2. For obtaining the required phase difference between adjacent patches, we adjust the lengths of the input and output transmission lines (each about half of the interconnecting lines between patches). By using the phase of S_{21}, we can adjust the lengths of the input and output transmission lines. This is done by using the following relation:

$$\beta l = -\alpha + \text{Ang}\,(S_{21}) \qquad (4\text{-}6)$$

We find the corresponding dimensions and the fraction of power loss in each chosen array element. These values are shown in Table 4-5. For a series-fed array without any load at the far end, the last element is a one-port patch and its design will not require any iteration.

The fractional power loss distribution associated with the nineteen element array is shown in Table 4-5. These values are inserted into subroutine PLOSS in program ARSYNT [7], which computes the new values of $|S_{21}|^2$ (which yield the required array amplitude distribution). These are shown in Table 4-6.

In the third step of the iteration procedure, the dimensions given in Table 4-5 are used as starting values to achieve the $|S_{21}|^2$ distribution of Table 4-6. This is done by slightly

Table 4-5

DESIGN DIMENSIONS AND ASSOCIATED POWER DISTRIBUTION OF ARRAY ELEMENTS WHOSE $|S_{21}|$ APPROXIMATE THE DISTRIBUTION OF TABLE 4-2

element #	approx· $\|S_{21}\|^2$	b(mm)	x_2(cm)	x_1(cm)	a(cm)	P_{loss}
1	.9671	1.00	.26	.255	1.485	.0278
2	.9662	1.00	.28	.276	1.483	.0284
3	.9651	1.00	.30	.295	1.481	.0292
4	.9639	1.00	.32	.315	1.479	.0299
5	.9523	1.50	.34	.332	1.439	.0363
6	.9323	2.50	.32	.307	1.3982	.0452
7	.9074	3.00	.36	.343	1.3800	.0570
8	.8798	3.25	.40	.381	1.3703	.0704
9	.8435	3.75	.42	.396	1.3588	.0864
10	.7976	4.25	.44	.410	1.3494	.1061
11	.7702	4.75	.44	.405	1.343	.1160
12	.7254	5.00	.46	.421	1.3389	.1351
13	.6869	5.00	.48	.438	1.3374	.1528
14	.6373	5.50	.486	.438	1.3321	.1713
15	.5867	5.75	.50	.445	1.3291	.1917
16	.5497	6.00	.506	.447	1.3268	.2056
17	.5229	6.25	.51	.445	1.3249	.2149
18	.4397	6.50	.53	.457	1.3221	.2481
19	0	6.5	0	.5045	1.3144	.4366

Table 4-6

$|S_{21}|^2$ DISTRIBUTION FOR EACH UNIT CELL FOR THE SECOND ITERATION

element #	$\|S_{21}\|^2$	element #	$\|S_{21}\|^2$
1	.9687	11	.7591
2	.9669	12	.7166
3	.9628	13	.6745
4	.9558	14	.6293
5	.9405	15	.5807
6	.9204	16	.5430
7	.8951	17	.5156
8	.8654	18	.4328
9	.8314	19	0
10	.7918		

Taylor 19 element array

S.L.L. = 30 dB, $N_A = 6$

changing the output port location x_2. It may be recalled that for a fixed width the value of $|S_{21}|$ decreases with increasing x_2 and vice versa. For a slight change in x_2, there will be a need for a small change in the values of a and x_1 to achieve $S_{11} = 0$. Table 4-7 shows the new power loss distributions as well as the elements' dimensions (a, b, x_1 and x_2) which yield the $|S_{21}|^2$ distribution of Table 4-5.

For elements with large width, the values of $|S_{21}|$ become very sensitive to the variation of the output port location x_2. (In these cases, x_2 values are shown with four digits compared to three digits for other elements.). At this stage of the iteration, there is no need to achieve very precise values for $|S_{21}|^2$, because the power loss (which is a critical parameter in the iteration process) depends very slightly on x_2.

Using the power loss distribution of Table 4-7 as input data to subroutine PLOSS, the new $|S_{21}|^2$ distribution along the array is computed. This distribution is shown in Table 4-8.

At this point in the iteration process, we can make a comparison between the $|S_{21}|^2$ distributions of Table 4-6 and Table 4-8. We see that $|S_{21}|^2$ remains the same for many elements. This shows that the iteration process is almost convergent. The last step of the iteration is to slightly change the value

Table 4-7

DESIGN DIMENSIONS AND ASSOCIATED POWER DISTRIBUTION
OF ARRAY ELEMENTS WHOSE $|S_{21}|$ APPROXIMATE
THE DISTRIBUTION OF TABLE 4-6

element #	$\|S_{21}\|^2$	b(cm)	x_2(cm)	x_1(cm)	a(cm)	P_{loss}
1	.9686	.100	.22	.215	1.491	.0268
2	.9669	.100	.26	.255	1.485	.0278
3	.9627	.125	.28	.274	1.463	.0302
4	.9548	.150	.32	.312	1.442	.0347
5	.9408	.200	.34	.330	1.4145	.0418
6	.9228	.250	.36	.346	1.394	.0505
7	.8946	.300	.390	.373	1.3770	.0638
8	.8668	.325	.420	.401	1.3683	.0772
9	.8340	.375	.430	.406	1.3579	.0912
10	.7955	.450	.430	.3980	1.3468	.1055
11	.7567	.500	.44	.4030	1.3404	.1207
12	.7183	.525	.455	.4140	1.3366	.1366
13	.6746	.55	.470	.4240	1.3332	.1546
14	.6294	.575	.483	.4317	1.3302	.1728
15	.5807	.600	.496	.4392	1.3274	.1921
16	.5395	.600	.51	.4500	1.3266	.2101
17	.5127	.625	.514	.448	1.3250	.2194
18	.4397	.650	.530	.4570	1.3221	.2481
19	0	.650	0	.5045	1.3144	.4366

of x_2 for the elements whose $|S_{21}|^2$ values in Table 4-8 are different from those in Table 4-6. The length of interconnecting transmission lines is now adjusted using equation (2-6). The final array dimensions are given in Tables 4-9 and 4-10.

4.5 Design of a Two-port Patch for a Given $|S_{21}|$:

In this section, we discuss the procedure for the computations of array elements' dimensions to achieve specified values of $|S_{21}|$ as well as to get $S_{11} = 0$. The specified value of $|S_{21}|$ for a particular patch is given by either equation 2-5 or 2-9. The transmission lines' lengths, L_1 and L_2, are to be computed using equation 2-6 where ℓ is replaced by $L_1 + L_2$. We have noticed that L_1 and L_2 should be at least $0.1\lambda_0$ in order to use just one external port at the end of the transmis sion line segment in the planar analysis. The design specifications are the operating frequency f(Hz) and the substrate specifications--the dielectric constant ε_r, the substrate height h, the dielectric loss tangent $\tan\delta$, and the strip thickness t. The transmission lines are specified in terms either of their characteristic impedances $Z_0(1)$, $Z_0(2)$ or their widths W_1, W_2 as shown in Figure 4-2.

The first step in the design of the two-port patch is to decide on an initial value of the patch width. As mentioned earlier, for high $|S_{21}|$ a narrow patch is chosen, and for low

Table 4-8

$|S_{21}|^2$ DISTRIBUTION FOR EACH UNIT CELL IN THE THIRD ITERATION

element #	$\|S_{21}\|^2$	element #	$\|S_{21}\|^2$
1	.9698	11	.7559
2	.9677	12	.7164
3	.9622	13	.6740
4	.9516	14	.6293
5	.9358	15	.5819
6	.9162	16	.5409
7	.8896	17	.5127
8	.8600	18	.4329
9	.8278	19	0
10	.7934		

Table 4-9

DESIGN OF 19 ELEMENT TAYLOR ARRAY SLL = 30

element #	a(cm)	b(cm)	x_2(cm)	x_1(cm)	P_{trans}	P_{rad}	P_{loss}
1	1.491	.100	.220	.215	.9686	.00457	.0268
2	1.4870	.100	.260	.255	.9671	.00504	.0278
3	1.4615	.125	.290	.284	.9609	.00736	.0317
4	1.4380	.150	.347	.339	.9514	.01171	.0368
5	1.4043	.225	.340	.329	.9345	.02075	.0447
6	1.3865	.275	.360	.345	.9152	.03098	.0537
7	1.3723	.325	.380	.361	.8905	.0445	.0649
8	1.3641	.350	.412	.391	.8613	.0598	.0787
9	1.3544	.400	.424	.398	.8278	.0791	.0928
10	1.3466	.450	.434	.402	.7915	.1008	.1075
11	1.3403	.500	.440	.403	.7566	.1224	.1208
12	1.3366	.525	.456	.414	.7173	.1453	.1371
13	1.3331	.55	.471	.4245	.6733	.1712	.1552
14	1.3301	.575	.484	.432	.6283	.1980	.1733
15	1.3274	.600	.496	.439	.5812	.2265	.1919
16	1.3252	.625	.503	.441	.5452	.2490	.2053
17	1.3233	.650	.508	.441	.5147	.2686	.2162
18	1.322	.650	.532	.458	.4337	.3150	.2507
19	1.3144	.650	0	.5045	0	.5624	.4366

Table 4-10

Design of a nineteen element Taylor array (continued)

element#	$\angle S_{21}$	$\angle V_e a_1$	$\angle V_e a_2$	ß l	l/ 2
1	-4.13	-1.86	177.97	265.57	1.1009
2	-3.96	-1.76	178.13	265.52	1.1007
3	-4.96	-2.27	177.67	264.64	1.0970
4	-5.81	-2.64	177.37	263.03	1.0904
5	-8.13	-3.88	176.18	261.09	1.0823
6	-9.55	-4.50	175.59	259.79	1.0769
7	-10.88	-5.11	175.04	258.69	1.0724
8	-11.51	-5.55	174.75	257.94	1.0693
9	-12.76	-6.08	174.27	256.74	1.0643
10	-14.10	-6.58	173.82	255.18	1.0578
11	-15.47	-7.30	173.18	254.36	1.0544
12	-16.18	-7.47	173.08	253.48	1.0508
13	-16.80	-7.70	172.95	253.09	1.0492
14	-17.58	-7.87	172.86	252.02	1.0447
15	-18.4	-8.27	172.57	251.30	1.0417
16	-19.31	-8.57	172.34	250.35	1.0378
17	-20.32	-8.91	172.05	250.04	1.0365
18	-20.46	-8.55	172.59	251.9	1.0442
19	0	-6.19	176.78	/	/

V_{e1} and V_{e2} are average phase angles between the input port and various points on the two radiating edges.

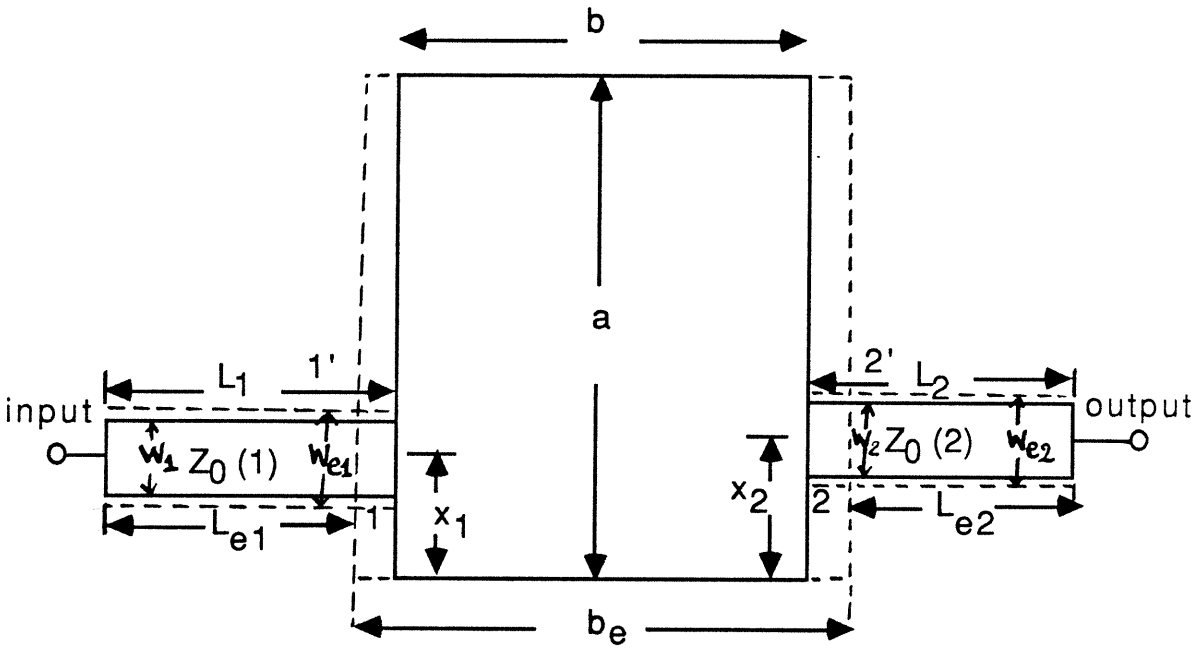

Fig. 4-2 Two port array unit cell showing effective dimensions

$|S_{21}|$ a wide patch is used. Using the approximate result [9],

$$|S_{21}| = \cos(\pi x_2 / a) / \cos(\pi x_1 / a) \qquad (4\text{-}8)$$

we notice that x_1 is always less than or equal to x_2 (because $|S_{21}| \leq 1$), where x_1 and x_2 are the input and output port distances from the closest radiating edge. (Input and output ports are assumed to be located on the side of the center line of the patch.) The difference between the values x_2 and x_1 is a function of the patch width, and it decreases with decreasing patch width. From the geometry of the rectangular patch, we note that $x_2 \leq a/2$ and $x_1 \geq w/2$, where w is the width of the transmission line connected to port 1. Also, for a given patch width there is a limited range of values of x_2 and x_1 for which $S_{11} = 0$.

For a given S_{21}, initial values of x_2 and x_1 are estimated from equation (4-8). The initial value of the patch length is approximated by

$$a \cong \frac{\lambda_0}{2\sqrt{\epsilon_{re}(f)}} \qquad (4\text{-}9)$$

where $\varepsilon_{re}(f)$ is the effective dielectric constant of the microstrip line of width b. These are used as starting values for the patch dimensions. An optimization procedure is then used to compute the final accurate design dimensions. This is done by fixing b and x_2 and varying the lengths a and x_1 to

get $S_{11} = 0$. In order to accelerate the optimization procedure, we start by using $N_C = 2$, $N_D = 2$, and twenty terms in the series summations (3.13) and (3.14). When the convergence is nearer, we take $N_C = 8$ and $N_D = 5$ and increase the number of terms in the summation to fifty.

An alternative method of obtaining the design dimensions is to use interactive iterations on the computer terminal. These are carried out by realizing that the real part of the input impedance (which should be equal to $Z_0(1)$ for input match) increases by increasing a (or by increasing x_1) and vice versa. On the other hand, the imaginary part of the input impedance (which should be equal to zero for input match) increases with decreasing x_1 (or increasing a). This procedure can be very efficient depending upon the starting values of a and x_1 in the iteration. These working rules have been arrived at by studying the variation of Z_{in} with parameter a and x_1 for two-port patches.

It may be noted that the input impedance is computed with reference to the effective input port location 1' (Fig. 4-2) because of the use of effective width b_e for the patch with a physical width b. The effective width is related to the characteristic impedance by

$$W_{eff}(f) = \frac{120 \cdot \pi \cdot h}{\sqrt{\epsilon_{re}(f)}\, Z(f)} \qquad (4\text{-}10)$$

where h is the substrate thickness, Z(f) is the characteristic impedance of the microstrip line of width b, and $\varepsilon_{re}(f)$ is the effective dielectric constant taking dispersion into account.

In Fig. 4-2, the effective lengths L_{e1} and L_{e2} are related to L_1, L_2 and to the effective width b_e of the patch of width b by

$$L_{e1,e2} = L_{1,2} - (b_e - b)/2 \qquad (4\text{-}11)$$

The design of a single-port patch also proceeds as above. In this case, the only fixed patch dimension is b. a and x_1 are varied to achieve $S_{11} = 0$.

The computations of the voltage along the radiating edges of the patches (when the second port is terminated in a matched load) is carried out by using equation (3-3) with the condition that

$$V_2 = -Z_0(2)\ I_2 \qquad (4\text{-}12)$$

This assumes that $S_{11} = 0$ for the next element also. Therefore,

$$V_E = [Z_V] \begin{pmatrix} 1 \\ \dfrac{-Z_c(2,1)}{Z_0(2) + Z_c(2,2)} \end{pmatrix} I_1 \qquad (4\text{-}13)$$

Elements of the matrix Z_c are given by equation (3-2), and I_1 is the current flowing at the input port 1. For a unit power delivered to the antenna input terminal by a source with $Z_s = Z_o(1)$, the input current is given by

$$|I_1|^2 = \frac{8Z_s}{|Z_s + Z_{in}|^2} \qquad (4\text{-}14)$$

where Z_{in} is the input impedance of the patch. The value of the voltages at the radiating edges given by (4-13) is used in Section 5 of this report to compute the radiation characteristics of the array.

4.6 Computation of Radiated Power:

The total power radiated by the patch is related to the voltage at the radiating edges by

$$P_{rad} = \sum_{i=1}^{N_c} \frac{G_R}{N_C} |V_E(i)|^2 \qquad (4\text{-}15)$$

where G_R is the radiation conductance of an edge, N_c is the total number of segments at the radiating edges, and $V_E(1)$, the value of the voltages at the i^{th} segment, are the elements of the vector V_E given in (4-13).

For a 1 watt input power delivered to the antenna input terminal, the net time average power fed to the array is

$$P_{in} = \frac{1}{2} \text{Real}(Z_{in}) \, |I_1|^2 \qquad (4\text{-}16)$$

For a two-port patch, the net time average power transmitted to the second port is

$$P_{rad} = |S_{21}|^2 \qquad (4\text{-}17)$$

The net time average power reflected at the antenna input is

$$P_{ref} = |S_{11}|^2 \qquad (4\text{-}18)$$

For a 1 watt input power, the power loss in the array (dielectric and conductor) is given by

$$\epsilon(i) = P_{in} - P_{trans} - P_{rad}(1 + \alpha') \qquad (4\text{-}19)$$

where α' is given by equation (3-8).

V. Computation of Radiation Characteristics

5.1 Array Factor:

For an array of identical radiating elements, the far field can be written as a product of the array factor and the radiation pattern of the individual elements. The array factor depends upon the elements' locations, phase distribution, and the excitation amplitudes for various elements. The array factor may be expressed as

$$F(\theta) = \sum_{n=1}^{N} C(n) \exp\{jn(k_0 d \cos\theta - \alpha)\} \qquad (5\text{-}1)$$

where d is the uniform interelement spacing, α is the uniform progressive phase in the array (which is related to the beam direction by (1-5)), C(n) is the relative amplitude excitation of the n^{th} element in the array, N is the number of elements in the array, and the angle θ is as shown in Fig. 5-1.

5.2 Radiation Pattern From Edge Voltages Distribution:

For the linear series-fed array of rectangular microstrip patches, the radiating elements are not identical, and therefore the array radiation characteristics cannot be computed by evaluating the array factor. In the present design procedure, the radiation pattern is obtained by first calculating the aperture field in the plane of the antenna and then evaluating the far-zone field by Kirchoff-Huygen's formula. Making use of the equivalence principle, the electric field distribution at the periphery of the patch is replaced by

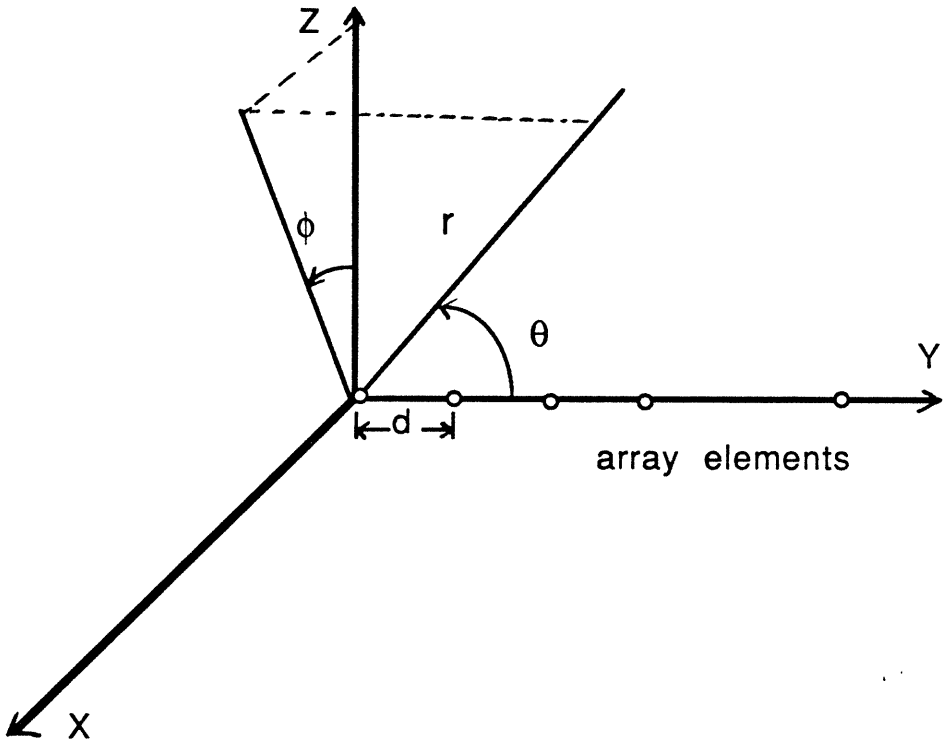

Fig 5-1 Linear array of isotropic elements with spherical coordinates being shown

an equivalent magnetic current line source as shown in Fig. 5-2. The magnetic density (in volts) of the line source is related to the voltage at the edges by

$$\overline{M} = \begin{cases} 2V\hat{y} & \text{for the left edge} \\ -2V\hat{y} & \text{for the right edge} \end{cases} \qquad (5\text{-}2)$$

where $\hat{y}$ is a unit vector in the y-direction. The factor 2 accounts for image of the magnetic current into the ground plane. The radiation is mainly from the the two edges of width b which are spaced distance a apart. The effect of the other two (non-radiating) edges can also be included if more accurate results or evaluation of the cross-polarization level is needed.

Each of the magnetic current line sources is divided into small sections over which the fields may be assumed to be uniform. These sections correspond to various ports on the radiating edges as considered in the segmentation method. The radiation field of the array is obtained by using the results of the radiation field of a linear magnetic current element as the building block.

5.2.1 Far Field of a Linear Magnetic Current Element:

The far field of a magnetic current line source located in the X-Y plane as shown in Fig. 5-3 is given by

$$E_\phi = -j2V_0Wk_0 \frac{e^{-jk_0r}}{4\pi r} F_L(\theta,\phi)$$

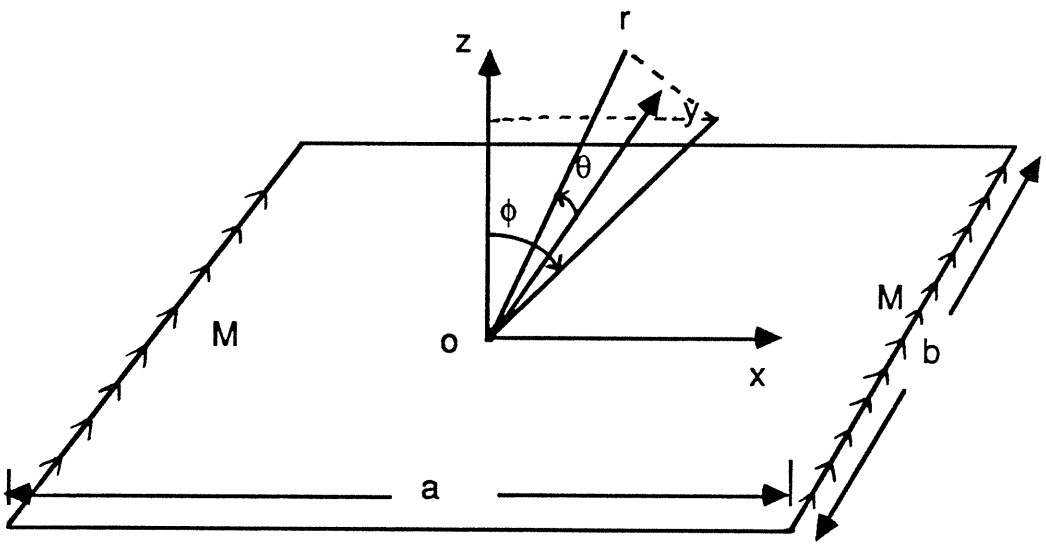

Fig 5-2 Equivalent magnetic line current at the radiating edges when the antenna is operating in the dominant mode.

(oa is the projection of or in the x-z plane)

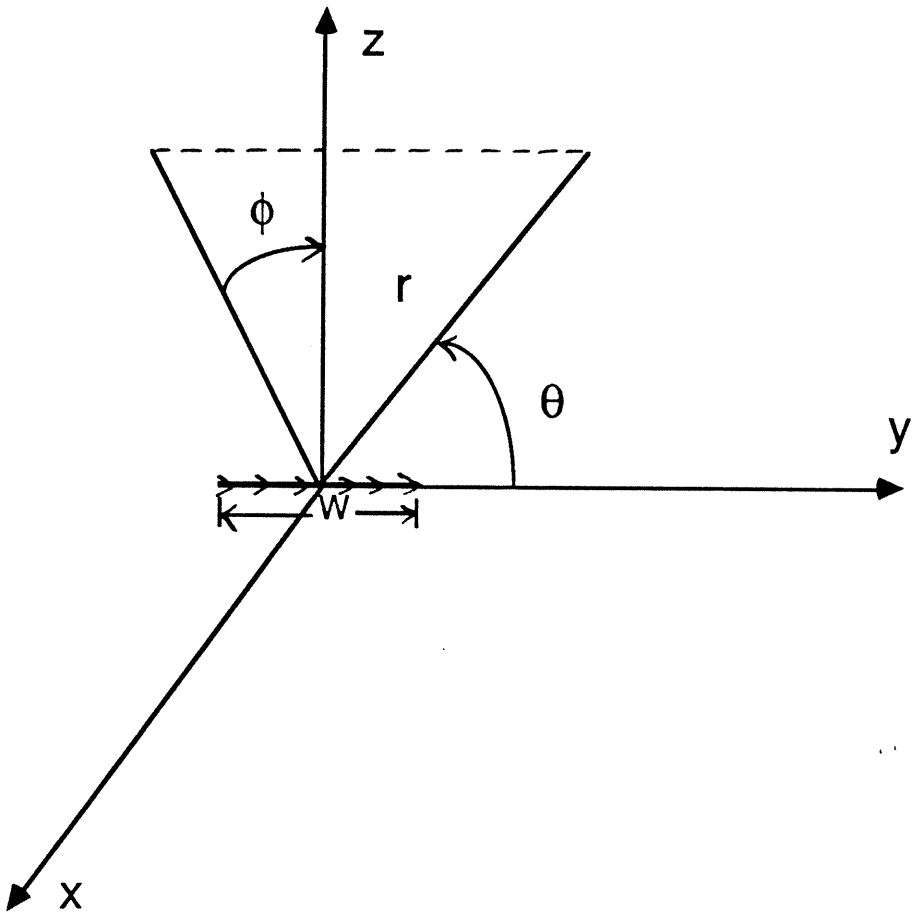

Fig. 5-3 Magnetic line source of length w parallel to the y-axis.

$$E_\theta = 0 \tag{5-3}$$

where

$$F_L(\theta,\phi) = \frac{\sin(\frac{k_0 w}{2}\cos\theta)}{\frac{k_0 w}{2}\cos\theta}\sin\theta$$

where V_0 is the magnitude of the magnetic current, which is taken to be uniform over its length, and W is the length of the magnetic current element.

The far field of a magnetic line source oriented arbitrarily in the X-Y plane (as shown in Fig. 5-4) is expressed as

$$\bar{E}_p = -2jV_0Wk_0\frac{e^{-jk_0r}}{4\pi r}e^{jk_0(x_0\sin\theta\sin\phi + y_0\cos\theta)}F(\theta',\phi')\bar{a}\phi' \tag{5-4}$$

where

$$F(\theta',\phi') = \frac{\sin(\frac{k_0 w}{2}\cos\theta')}{\frac{k_0 w}{2}\cos\theta'}\sin\theta'$$

and where

$$\mathbf{a}_\phi' = \Phi_\phi\mathbf{a}_\phi + \Phi_\theta\mathbf{a}_\theta \tag{5-5}$$

$$\Phi_\phi = \sin\phi'\sin\phi + \cos\delta\cos\phi\cos\phi'$$

$$\Phi_\theta = -\sin\phi'\cos\theta\cos\phi + \cos\delta\cos\theta\sin\phi + \sin\delta\cos\phi'\sin\theta$$

$$\cos\theta' = \sin\theta\sin\phi\sin\delta + \cos\theta\cos\delta \tag{5-6}$$

$$\cos\phi' = \sin\theta\cos\phi \,/\, \sqrt{1 - \cos^2\theta'}$$

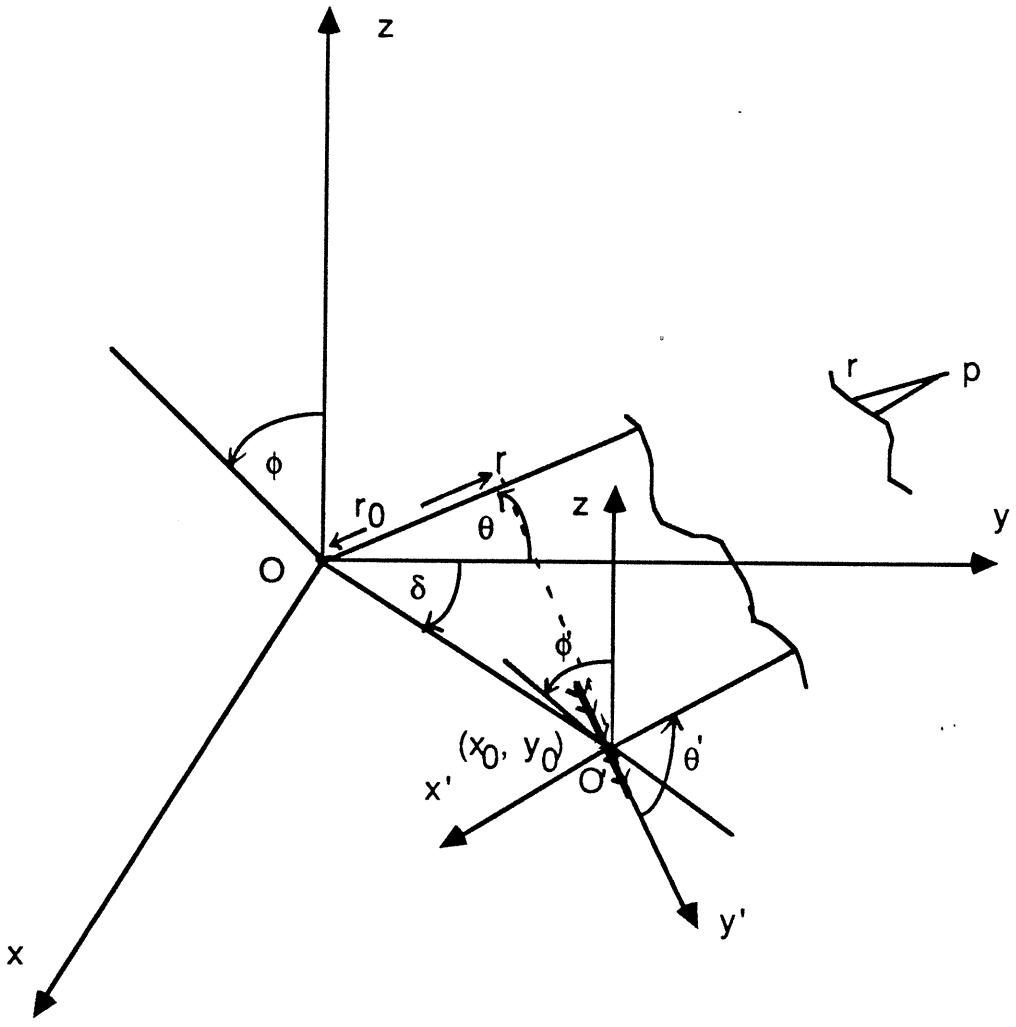

Fig. 5-4 Far field of an arbitrarily oriented linear magnetic current in the x-y plane

5.2.2 Far Field of a Rectangular Microstrip Patch:

When the rectangular patch is operating in the dominant mode, the voltages at the two radiating edges are equal in magnitude and are 180° out of phase. In this case, the far field pattern of the rectangular patch shown in Fig. 5-2 is given by

(5-7)

$$F(\theta,\phi) = \begin{cases} \cos\left(\frac{k_0 a}{2}\sin\phi\right), & \text{E-plane } (\theta = \pi/2) \\ \dfrac{\sin\left(\frac{k_0 b}{2}\cos\theta\right)}{\frac{k_0 b}{2}\cos\theta}\sin\theta, & \text{H-plane } (\phi = 0) \end{cases}$$

When the antenna is operating slightly out of resonance, the voltages at the radiating edges are not uniform. Each radiating edge is divided into $N_c/2$ segments (as discussed in Section 3.3). The voltage along the width of each segment is taken to be uniform. The radiation characteristic of the patch is then computed using the superposition of the far field radiated by each segment. The far field pattern of the rectangular patch is given by

(5-8)

$$F_p(\theta,\phi) = \sum_{i=1}^{N_c} V_0(i)\, W(i)\, \exp\{j(k_0 r_0(i) + \alpha(i)\}F_i(\theta,\phi)$$

where

(5-9)

$$F_i(\theta,\phi) = \frac{\sin\left(\frac{k_0 W(i)}{2}\cos\theta\right)}{\frac{k_0 W(i)}{2}\cos\theta}\sin\theta$$

$V_0(i)$, $\alpha(i)$ are the magnitude and relative phase (with reference to the input signal) of the voltage at the i^{th} edge section of width w(i). N_c is the number of segments at the two radiating edges.

$$r_0(i) = x_0(i) \sin(\theta) \sin(\phi) + y_0(i) \cos(\theta) \tag{5-10}$$

$(x_0(i), y_0(i))$ is the coordinate location of the i^{th} segment relative to the coordinate system (x,y,z) as shown in Fig. 5-2.

5.2.3 Radiation Characteristic of a Series-fed Array:

In this section, we will discuss the computation of the far field pattern of the series-fed array considered in this report. The array is fed in series from one of the ends. The far field pattern of the array of Fig. 5-5 is given by

$$F_T(\theta,\phi) = \sum_{d=1}^{N} F_E^j(\theta,\phi) \tag{5-11}$$

where

$$F_E^j(\theta,\phi) = \sum_{i=1}^{N_c} V_0(i,j)\ W(i,j)\ e^{j(k_0 r_0(i,j) + \alpha(i,j))}\ F_{L(i,j)}(\theta,\phi) \tag{5-12}$$

where

$$F_{L(i,j)}(\theta,\phi) = \frac{\sin\left(\frac{k_0 W(i,j)}{2}\cos\theta\right)}{\frac{k_0 W(i,j)}{2}\cos\theta}\sin\theta \tag{5-13}$$

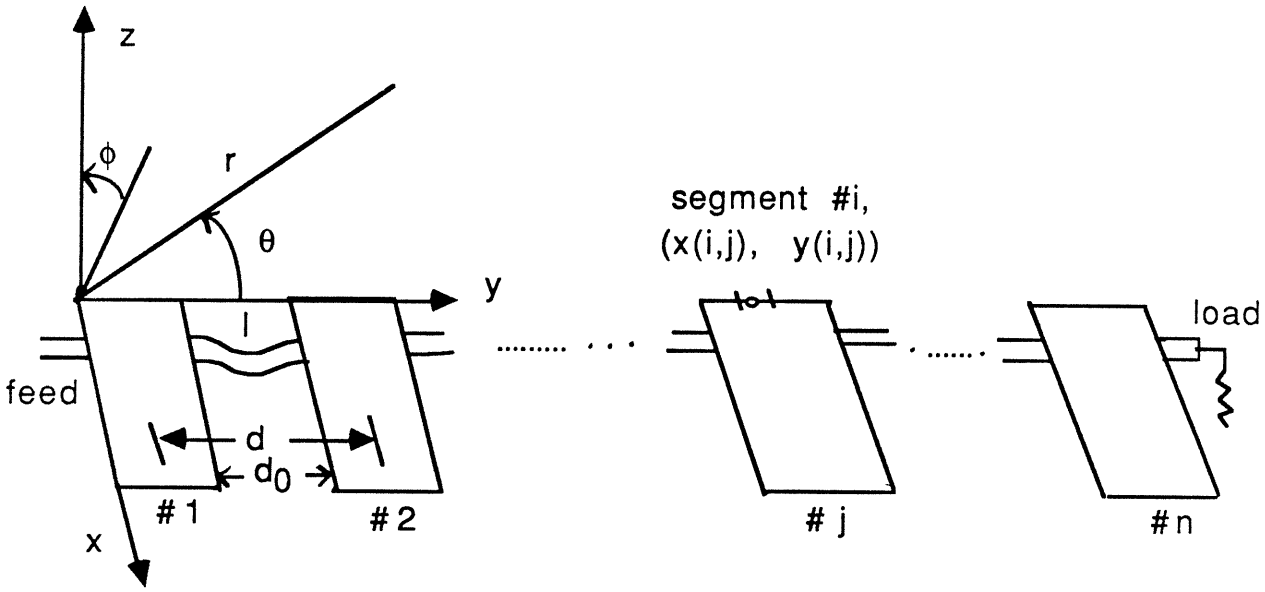

Fig. 5-5 Series fed linear array of rectangular microstrip patches

and

$$r_0(i,j) = x_0(i,j)\sin\theta\sin\phi + y_0(i,j)\cos\theta \qquad (5\text{-}14)$$

$V_0(i,j)$ and $\alpha(i,j)$ are the voltage's magnitude and relative phase of i^{th} segment in the j^{th} radiating array element. $(x(i,j), y(i,j))$ are the coordinate locations of the i^{th} segment (of width $w(i,j)$) of the j^{th} array element.

Once the voltage distribution and the location of the segments are obtained, the computation of the radiation pattern is carried out using relations (5-11) through (5-14).

5.2.4 Computation of Voltage Distribution:

The voltage distribution at the radiating edges of the array elements is computed by use of the segmentation method. Figure 5-6 shows a series-fed linear array consisting of N unit cells. Each unit cell is characterized by an impedance matrix Z_C with respect to the external ports. For a one-port cell or for the load (connected to the end of the array), the impedance matrix reduces to the input impedance of the one-port cell and the value of the load respectively. Each unit cell is also characterized by a voltage matrix Z_V which relates the voltages at the radiating edges to the currents flowing into the external ports of the unit cell. Once the port currents are determined, the voltage distribution at the edges can be found. Application of the segmentation method [4, p. 353] for computing edge voltages is discussed in this

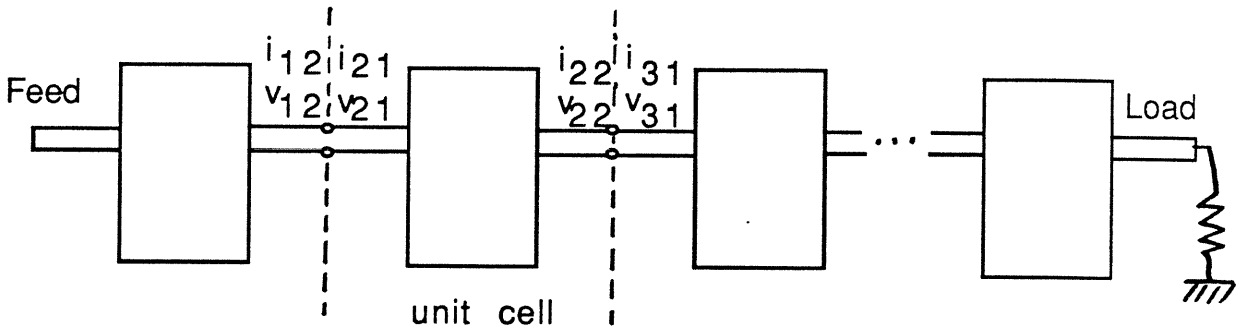

Fig 5-6 Linear series fed array of N unit cells.

section.

For the implementation of the segmentation method, the voltage and current variables for all of the unit cells may be expressed as

$$\begin{bmatrix} V_p \\ V_c \end{bmatrix} = \begin{bmatrix} Z_{pp} Z_{pc} \\ Z_{cp} Z_{cc} \end{bmatrix} \begin{bmatrix} I_p \\ I_c \end{bmatrix} \tag{5-15}$$

where V_p and I_p are the voltage and the current at the input of the array (p=1). V_c and I_c are the voltages and currents at the connected ports. The number of connected ports is equal to (N-1) for an array without load and is equal to N (the number of elements) for an array terminated by a matched load.

The constraints imposed upon the voltage and current at the connected ports are:

(i) voltages at the two connected ports are equal

(ii) currents at two connected ports are equal in magnitude, and their sum is zero.

For all of the internal ports, the constraint matrices are written as

$$\Gamma_1 V_c = 0, \ \Gamma_2 I_c = 0 \tag{5-16}$$

Γ_1 and Γ_2 are matrices with c/2 rows and c columns. Each matrix row describes a connection constraint, and the elements of every row are zero except for the two elements corresponding to the connected ports. The values of the

non-zero elements are1 or -1 for the matrix Γ_1 and 1 for all non-zero elements of the matrix Γ_2. Using equations (5-15) and (5-16), the currents at the connected ports are expressed as

$$I_c = \begin{bmatrix} \Gamma_1 Z_{cc} \\ j\Gamma_2 \end{bmatrix}^{-1} \begin{bmatrix} -\Gamma_1 Z_{cp} \\ 0 \end{bmatrix} i_p \qquad (5\text{-}17)$$

The analysis also yields the input impedance of the array, which is given by

$$Z_p = Z_{pp} - Z_{pc} \begin{bmatrix} \Gamma_1 Z_{cc} \\ j\Gamma_2 \end{bmatrix}^{-1} \begin{bmatrix} -\Gamma_1 Z_{cp} \\ 0 \end{bmatrix} \qquad (5\text{-}18)$$

The currents I_c at the connected ports (given by equation 5-17) are evaluated by considering a unit input current at the feed point. The voltages at the radiating edges are then calculated by use of the matrix Z_V.

Subroutine SENSV4 in [7] is used for the computation of the voltage distribution at the radiating edges and also the input impedance of the array.

5.2.5 Computation of Segment Location:

The coordinates (x, y) of the center points of various segments, are computed from the array configuration. It may be recalled that the elements are not identical (i.e, they have different dimensions). As discussed later in Section 6, the

array is laid out in such a way that the radiating edges nearer to the input and output ports are made colinear. The other edges will not be necessarily colinear. In this case, the coordinates of the center points of the segments in the (x,y,z) system of coordinates shown in Fig. 5-5 are x(i,j) = 0 for segments (i^{th} segment of the j^{th} element) at the radiating edges nearer to the input transmission lines and x(i,j) = a(j) otherwise. Also,

$$y(i,j) = b(i)\,(2i-1)\,/\,2N_c + \sum_{k=1}^{j-1} (b(k) + d_0) \qquad (5\text{-}19)$$

where b(i) and a(i) are the patch width and length respectively of the i^{th} patch, d_0 is the uniform edge to edge spacing between elements, and N_C is the number of segments at the two radiating edges of a patch. (N_C is taken to be the same for all patches.)

Program PATV4 listed in [7] is used to compute the far field pattern of the series fed linear array by making use of relations (5-11) through (5-19).

5.3 A Numerical Example:

As an example of the use of the procedure discussed in Sections 5.1 and 5.2, consider the case of the nineteen element linear series-fed array of Section 4.4. Figure 5-7 shows the array factor obtained from equation (5-1) with

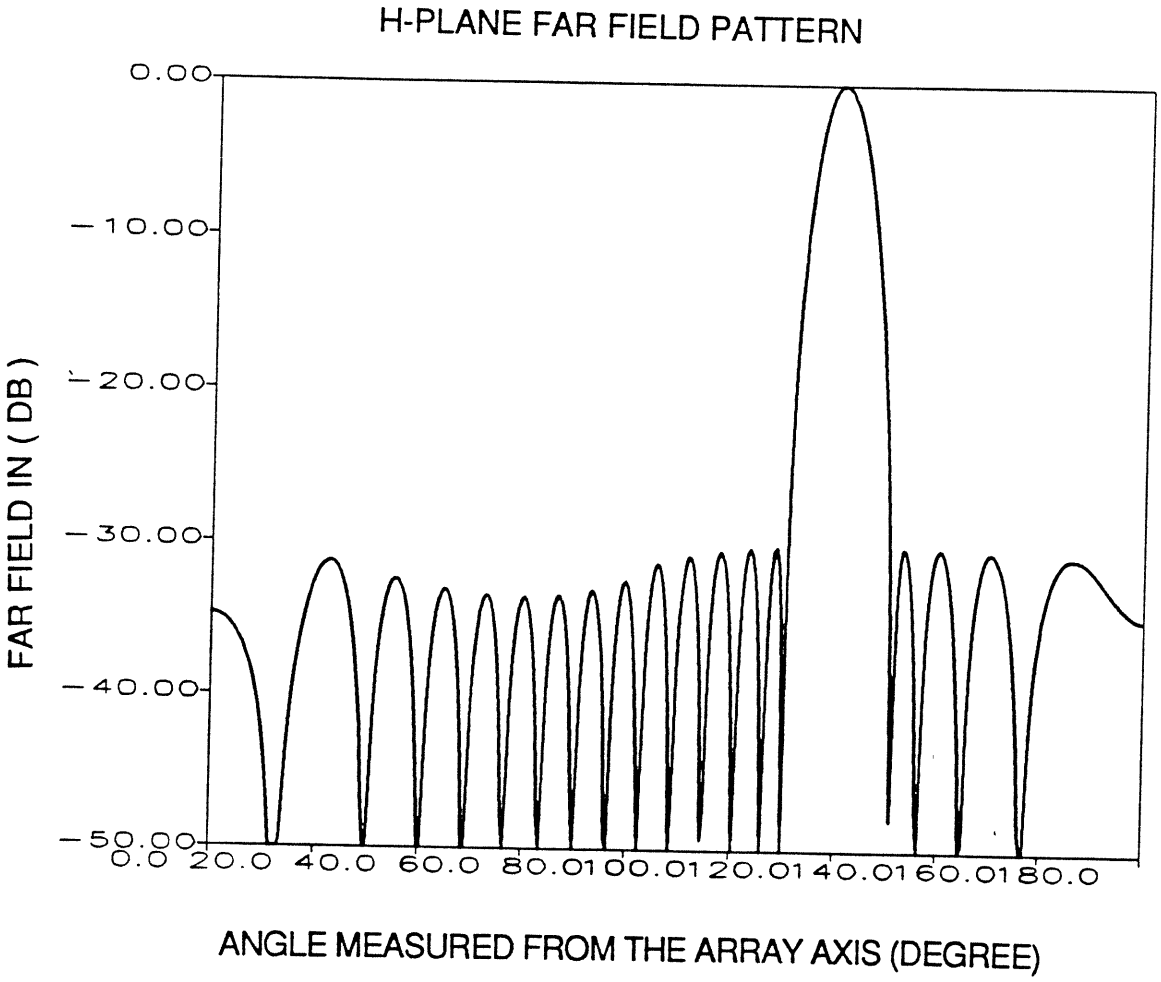

Fig 5-7 Array factor for a 19 element TAYLOR array computed using equation (5-1).

$k_0 d = \pi$, $\alpha = -270°$.

Figure 5-8 shows the far field pattern by using the analysis of Section 5.2. We notice changes in the level of side lobes due to the non-identical element patterns for various elements in the array. Aside from this, the agreement between Fig. 5-7 and Fig. 5-8 is acceptable. These plots show that the effect of the voltage non-uniformity may be ignored for computing the SLL. However, the element pattern given by equation (5-7) may cause the beam direction to shift considerably if the array is scanned near the endfire.

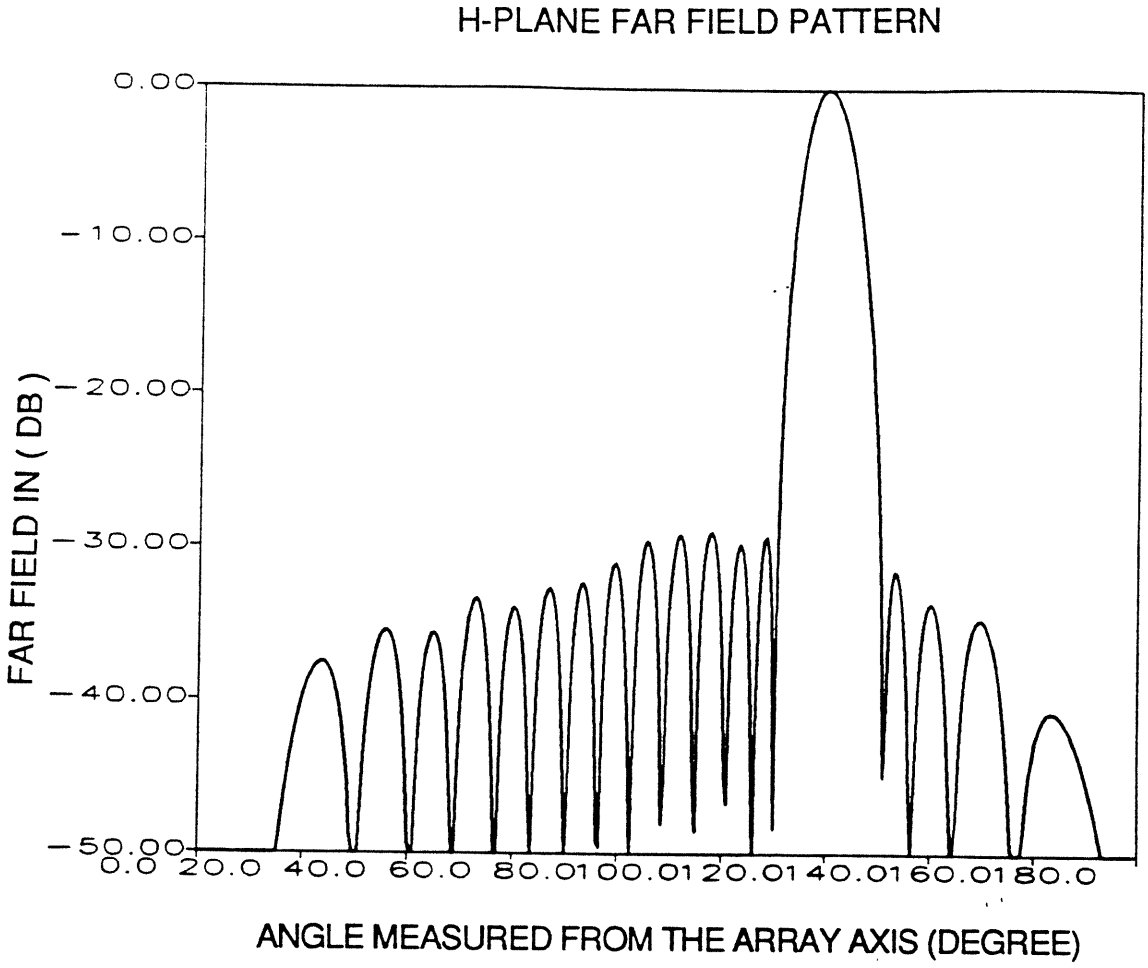

Fig. 5-8 Far field pattern of 19 element series fed array computed using the voltage distribution along the radiating edges.

VI. Array Layout

In this section, we describe a method for layout of the linear series-fed array analyzed and designed in the previous chapter. This section constitutes the last step in array design before it is fabricated.

As discussed earlier, the array elements do not have equal lengths, and the radiating edges which are nearer to the input and output transmission lines are made colinear. The other edges will not necessarily be colinear. For a fixed uniform spacing between adjacent array elements, the interelement transmission lines have to be curved to fit in the spacing between the elements as shown in Fig. 6-1. To reduce the effect of curvature (reflection and radiation), the bending should be very smooth. Also, for minimizing the junction reactances the transmission lines should be perpendicular to the patch at the junction points. This reduces the effect of feed discontinuity and allows the segmentation method to be used conveniently. The layout of the curved interconnecting lines used in the present design is shown in Fig. 6-1. The different parameters in Fig. 6-1 are related to the array dimensions as follows:

$$L_T = 4\, r\, \theta \tag{6-1}$$

$$S^2 = d'_i{}^2 + \Delta_i^2 \tag{6-2}$$

$$S = 4r \sin\theta \tag{6-3}$$

where r is the radius of the circular bending, θ is the arc angle, and

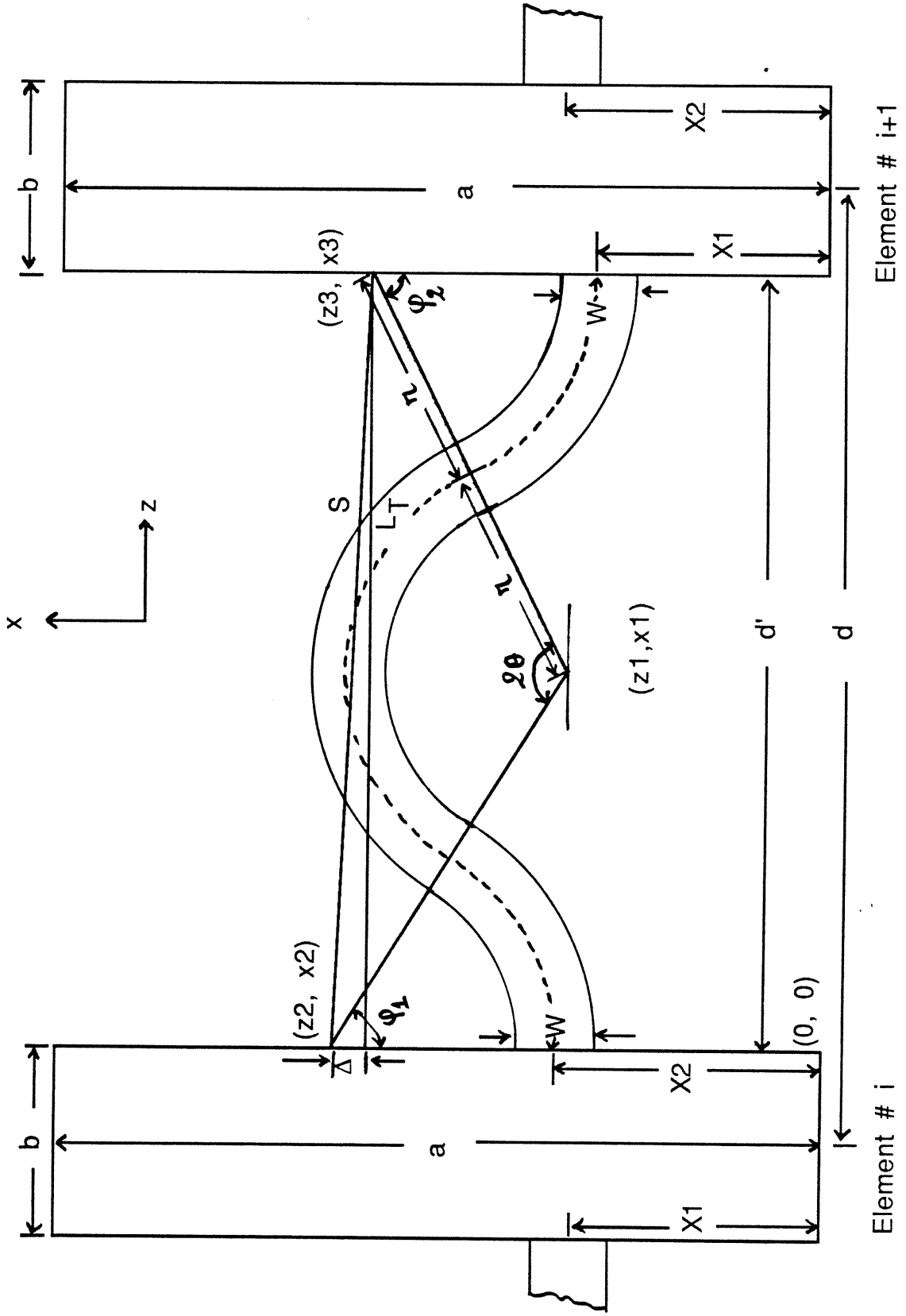

Fig. 6-1 Layout of two adjacent array elements.

d'_i is the interelement spacing (edge to edge as shown in Fig. 6-1). This spacing is related to the uniform element spacing d by

$$d'_i = d - (b_i + b_{i+1})/2 \tag{6-4}$$

where b_i is the width of the i^{th} array element. Δ_i is the offset between the output port location $x_2(i)$ of the i^{th} element and the input port location $x_1(i+1)$ of the $(i+1)^{th}$ element. We have

$$\Delta_i = X_2(i) - X_1(i+1) \tag{6-5}$$

L_T is the transmission line length connecting the i^{th} element to the $(i+1)^{th}$ element in the array.

Using (6-1) through (6-3), we get a transcendental equation to determine θ. This is given by

$$\theta = \frac{L_T}{\sqrt{d'^2_i + \Delta^2_i}} \sin(\theta) \tag{6-6}$$

and r will be given by

$$r = L_T/4\theta \tag{6-7}$$

The other geometrical parameters shown in Fig. 6-1 are related to θ, r, x_2, x_1 by

$$z_1 = 2r \sin(\theta - \Psi) \qquad x_1 = r + x_2 - 2r \cos(\theta - \Psi)$$

$z_2 = 0 \quad x_2 = r + x_2$

(6-8)

$z_3 = d_i$ $\qquad$ $x_3 = r + x_1$

$\Phi_1 = 90° - \theta + \Psi$ $\qquad$ $\Phi_2 = 90° - \theta - \Psi$

where $\tan(\Psi) = \Delta_i / d'_i$.

Equations (6-1) through (6-8) are used to lay out the linear series-fed array.

Appendix A

Formulas for Microstrip transmission Line Design:

In this appendix, different design formulas to compute the transmission line characteristic parameters Z_0, ϵ_{re}, and we as a function of transmission line width are given [11].

a) Impedance and Effective Dielectric Constant for a Given Width:

$$Z_{01}(u) = \frac{\eta_0}{2\pi} \ln\left[\frac{f(u)}{u} + \sqrt{1+\left(\frac{2}{u}\right)^2}\right], \quad u = w/h \tag{1}$$

$$f(u) = 6 + (2\pi - 6)\exp\left[-\left(\frac{30.666}{u}\right)^{0.7528}\right], \quad \eta_0 = 120\pi r \tag{2}$$

--accuracy $\leq$ 0.01% for $u \leq 1$ and 0.03% for $u \leq 1000$.

$$\epsilon_e(u,\epsilon_r) = \frac{\epsilon_r + 1}{2} + \frac{\epsilon_r - 1}{2}\left(1 + \frac{10}{u}\right)^{-a(u)b(\epsilon_r)} \tag{3}$$

$$a(u) = 1 + \frac{1}{49}\ln\frac{u^4 + (u/52)^2}{u^4 + 0.432} + \frac{1}{18.7}\ln\left[1 + \left(\frac{u}{18.1}\right)^3\right] \tag{4}$$

$$b(\epsilon_r) = 0.564\left(\frac{\epsilon_r - 0.9}{\epsilon_r + 3}\right)^{0.053} \tag{5}$$

--accuracy $\leq$ 0.2% for $\epsilon_r \leq 128$ and $0.01 \leq u \leq 100$.

b) Strip Thickness Correction:

$$\Delta u_1 = \frac{T}{\pi} \ln\left(1 + \frac{4 \exp(1)}{T \coth^2 \sqrt{6.517u}}\right), \qquad T = t/h \tag{6}$$

where t is the thickness of the conducting strip.

$$\Delta u_r = \frac{1}{2}\left(1 + 1/\cosh \sqrt{\epsilon_r - 1}\right)\Delta u_1 \tag{7}$$

$$u = u + \Delta u, \qquad u_r = u + \Delta u_r$$

$$Z_0(u,t,\epsilon_r) = Z_{01}(u_r)/\sqrt{\epsilon_e(u_r,\epsilon_r)} \tag{8}$$

$$\epsilon_{eff}(u,t,\epsilon_r) = \epsilon_r(u_r,\epsilon_r)[Z_{01}(u_1)/Z_{01}(u_r)] \tag{9}$$

c) Dispersion Correction:

$$\epsilon_{eff} = \epsilon_r - \frac{\epsilon_r - \epsilon_{eff}(o)}{1 + G(f/f_p)^2}, \qquad f_p = Z_0/2\mu_0 h \tag{10}$$

where h is the substrate thickness

$$G = \frac{\pi^2}{12} \frac{\epsilon_r - 1}{\epsilon_{eff}(o)} \sqrt{\frac{2\pi Z_0}{\eta_0}}, \qquad f_p = Z_0/2\mu_0 h \tag{11}$$

$$Z_0(f) = Z_0(0) \sqrt{\frac{\epsilon_{eff}(o)}{\epsilon_{eff}(f)}} \frac{\epsilon_{eff}(f) - 1}{\epsilon_{eff}(0) - 1} \tag{12}$$

d) Computation of Width from Impedance [4]:

For A < 1.52:

$$w/h = \frac{8\exp(A)}{\exp(2A) - 2} \tag{13}$$

For $A \leq 1.52$:

$$w/h = \frac{2}{\pi}\left\{B - 1 - \ln(2B - 1) + \frac{\epsilon_r - 1}{2\epsilon_r}\left[\ln(B - 1) + 0.39 - \frac{0.61}{\epsilon_r}\right]\right\} \tag{14}$$

where

$$A = \frac{Z_0}{60}\left(\frac{\epsilon_r + 1}{2}\right)^{1/2} + \frac{\epsilon_r - 1}{\epsilon_r + 1}\left(0.23 + \frac{0.11}{\epsilon_r}\right)$$

$$B = \frac{60\pi^2}{Z_0\sqrt{\epsilon_r}}$$

REFERENCES

1. R. S. Elliot, *Antenna Theory and Design*, (Englewood Cliffs, NJ: Prentice-Hall)1981.

2. C. A. Balanis, *Antenna Theory: Analysis and Design*, (New York: Harper and Row) 1982.

3. J. R. James, et al., *Microstrip Antenna Theory and Design*, (Stevenage, UK: Peter Peregrinus) 1981.

4. K. C. Gupta, et al., *Computer-Aided Design of Microwave Circuits*, (Delham, MA.: Artech House, Inc.) 1981.

5. A. Benalla and K. C. Gupta, "Faster Computation of Z-Matrices for Rectangular Segments in Planar Microstrip Circuits," *IEEE Trans*, MTT-**34**, June 1986, pp. 733-736.

6. A. Benalla and K. C. Gupta, "Two-Dimensional Analysis of One-Port and Two-Port Rectangular Microstrip Antennas," E. M. Lab, Sci. Rep. 85, Univ. of Colorado, Boulder, May 1986.

7. A. Benalla, "Computer Aided Design of Series-Fed Linear Array of Rectangular Microstrip Patches," Software Doc. Rep., SDR1, Dept. of ECE, Univ. of Colorado, Boulder, Sept. 1987.

8. I. Wolff and N. Knoppik, "Rectangular and Circular Microstrip Disc Capacitors and Resonators," *IEEE Trans*, MTT-**22**, 1974, pp. 857-864.

9. K. C. Gupta, "Two-Port Transmission Characteristics of Rectangular Microstrip Patch Radiators," *IEEE AP-S International Sym, Vancover BC, Digest*, 1985, pp. 71-74.

10. A. Benalla and K.C. Gupta, "Multiport Network Model for Mutual Coupling in Microstrip Patches," (to be published).

11. E. Hammersted and O. Jensen, "Accurate Models for Microstrip Computer-Aided Design," *IEEE MTT-S International Microwave Symposuim, Digest*, 1985, pp. 407-409.